AN EXPERIMENTAL STUDY OF THE EFFECTS OF SURFACE ROUGHNESS AND SURFACTANT ON POOL BOILING OF NANOFLUIDS

AN EXPERIMENTAL STUDY OF THE EFFECTS OF SURFACE ROUGHNESS AND SURFACTANT ON POOL BOILING OF NANOFLUIDS

By

Mohamed Hamda, B. Sc.

A Thesis

Submitted to the School of Graduate Studies

In Partial Fulfilment of the Requirements

For the Degree

Master of Applied Sciences

McMaster University

Hamilton, Ontario, Canada

MASTERS OF APPLIED SCIENCES (2015) McMaster University
(Mechanical Engineering) Hamilton, Ontario, Canada

TITLE: An Experimental Study Of The Effects Of Surface Roughness And Surfactant On Pool Boiling Of Nanofluids

AUTHOR: Mohamed Hamda, B. Sc. (Alexandria University)
SUPERVISOR: Dr. Mohamed Hamed
NUMBER OF PAGES: xiii, 91

Abstract

The use of nanofluids as heat transfer fluids has received a lot of attention from the heat transfer research community. Due to the increased thermal conductivity of nanofluids over their base fluids, the number of nanofluids scientific publications increased significantly in the past decade. The effects of the heated surface roughness, nanoparticles and surfactant concentrations on pool boiling of nanofluids have been thoroughly investigated. However, contradicting findings have been observed under what appeared to similar test conditions.

In this experimental investigation, two boiling surfaces have been prepared with an average surface roughness of 6 and 60 nm using high precision machining. Alumina Oxide-Water based nanofluids have been used in this investigation. The initial nanoparticle size reported by the manufacturer is 10 nm. The nanoparticles concentration has been kept at 0.05 wt. %. A Sodium Dodecylbenzenesulfonate (SDBS) surfactant has been added to the nanofluids in order to improve its stability. Results showed that the nanofluids boiling performance depended on the boiling surface roughness. The heat transfer coefficient (HTC) obtained in the case of the smooth, mirror finished surface showed an enhancement of 205% with respect to pure water. This trend was reversed in the case of the rough surface which is believed to be due to significant nanoparticles deposition. The HTC obtained with the rough surface was 12% lower than that of pure water. The effect of the surfactant concentration on nanoparticles deposition has been investigated by changing the surfactant concentration from 0.1 to 1.0 wt. %. In the case of the rough surface, the increase of surfactant concentration was found to reduce the formation of the nanoparticles deposition layer. The HTC obtained with the higher surfactant concentration was increased by 46 %.

The effect of nanoparticles concentration on the smooth surface shows an unexpected trend of 20 % reduction of the transfer rate of the nanofluids coupled with the increase of the nanoparticle concentration from 0.05 to 0.1 wt. %. However all concentrations showed heat transfer enhancement with respect to pure water. The minimum heat transfer coefficient ratio enhancement was 11 % using 0.1 wt. % nanofluids with respect to pure water.

Since nanoparticles deposition has been observed and attributed to micro-layer evaporation, an investigation has been carried out to examine the nucleation process during the pure water and nanofluids pool boiling. The bubble growth rate in both cases was analyzed at different wall degrees of superheat ranging from 104.3 to 105.9 ºC. In addition, the bubble departure diameter and frequency have been measured and compared for both cases. The nanofluid bubble size was about 80 % smaller than that of pure water. The nanofluid bubble departure had almost constant frequency of 500 Hz over the range of wall superheats whereas the maximum bubble frequency in the case of pure water was 22.72 Hz.

Acknowledgement

I would like to thank my supervisor Dr. Mohamed Hamed for his guidance, support and encouragement.

I would like to thank all my colleagues who made this Masters a memorable experience. Nayef Almalki, Omar Aljammal, Mohamed Yasser, Ayman Farid, Mostafa Morsy, Mostafa Medra, Taib Arif, Alex, Mohammed Tawhid, you guys have been awesome.

Last but not least, special thanks to all my family members and friends back home for their continuous support. Without them I would not have made it this far.

Table of Contents

List of Figures

List of Tables

Nomenclature

Symbol	Description	Units
k	Thermal Conductivity	KW/(m.K)
σ	Surface Tension	N/m
r_{nuc}	Nucleation Radius	mm
ΔT_{nuc}	Nucleation Superheat	ºC
p	Pressure	Pa
φ	Heterogeneous nucleation factor	-
β	Contact Angle	º
$\acute{\beta}$	Apparent Contact Angle	º
θ	Included Angle	º
R	Bubble instantaneous radius	cm
t	Time	sec
R^+	Non dimensionalized radius	-
t^+	Non dimensionalized time	-
T_f	Liquid temperature	ºC
P_f	Liquid pressure	Pa
T_{sat}	Liquid saturation temperature	ºC
P_{sat}	Saturation pressure	Pa
h_{fg}	Latent heat of vaporization	J/Kg
ρ_g	Vapor density	Kg/m^3
ρ_f	Liquid density	Kg/m^3
Ja	Jacob number	-
SDBS	Sodium dodecylbenzenesulfonate	-
HTC	Heat transfer coefficient	KW/m^{2}K
ONB	Onset of nucleate boiling	-
CHF	Critical heat flux	-
CuO	Copper oxide	-
Al_2O_3	Alumina oxide	-
CMC	Critical Micelle Concentration	mg/l
Na	Sodium	-
TPS	Transient plane source	-
pH	Acidity scale	-
IEP	Isoelectric point	
ZrO_2	Zirconium oxide	
TMAH	Tetramethyl ammonium hydroxide	-

SDS	Sodium dodecyl sulfate	-
SIP	Surface Interaction Parameter	-
Ra	Average surface roughness	nm
EBL	Electron beam lithography	-
ITO	Indium tin oxide	-
IR	Infra-red	-
HSV	High Speed Video	-
PID	Proportional integral derivative	-
RTD	Resistance temperature detector	
DLS	Dynamic light scattering	-
EDM	Electric discharge machining	-
NP	Nanoparticles	-

Chapter 1 Introduction

Heat transfer enhancement has received significant attention in the last few decades as a result of the significant technological advancement in various technologies such as power electronics and material processing. In these applications, efficient means of extracting large amounts of heat required.

Among different heat transfer mechanisms, boiling heat transfer possessed the highest heat transfer rate with respect to other heat transfer mechanisms. It is clearly seen by comparing the values of heat transfer coefficient from various heat transfer mechanisms.

- Free Convection: 20 – 100 $\frac{W}{m^2K}$
- Forced Convection: 50 – 10.000 $\frac{W}{m^2K}$
- Boiling: 3.000 – 100.000 $\frac{W}{m^2K}$

Not only are these values limited to the convection mechanism but also the working fluid applied. These conventional working fluids such as water, oil and ethyl glycol have very low thermal conductivity compared to those of solids. Table 1.1 shows the values of the thermal conductivity of different solids and fluids. It is clear that the thermal conductivity of fluids is two or three orders of magnitude less than that of the solids. Therefore, the thermal conductivity of liquids is considered the source of the largest resistance in heat exchanger effectiveness.

Table 1.1: Thermal conductivity of different substances.

Substance	Thermal Conductivity, k, $\frac{KW}{m.K}$
Engine Oil	0.15
Alcohol	0.17
Water	0.58
Steel, Carbon 1%	43
Aluminum	205
Copper	401

Scientists attempted to increase the thermal conductivity of fluids by using homogenous suspension of small metal particles in base fluids. Maxwell [1] developed a model proposing that the effective thermal conductivity of the new mixture will increase with the volume fraction of the solid particles as well as the ratio of the surface area to volume of the particles. The particles were limited to millimeter size scale. However, these new fluids were not practical to use as the stability of the particles were too low and they caused severe clogging problems. With advancements in manufacturing technologies, the particles were reduced to the nanometer size scale, referred to as nanoparticles. In this chapter, a brief discussion about pool boiling and its different regimes is presented followed by a review of nanofluids.

1.1 Pool Boiling

Pool boiling occurs at the solid liquid interface when its temperature exceeds the liquid's saturation temperature. Bulk fluid remains stagnant during pool boiling. However, fluid experiences motion due to wall heat convection and disturbance caused by bubble growth and coalescence. The boiling curve shows the variation in heat flux at different levels of wall superheat, which is the difference between the surface and saturation temperatures. The first boiling curve was introduced by Nukiyama in 1934 for the pool boiling of water. As shown in Figure 1.1, the heat flux experiences dramatic changes with the continuous increase of the wall superheat that the heat transfer can be divided into four distinct regimes.

1.1.1 Single Phase Natural Convection Regime

Heat is purely removed from the solid surface by natural convection, and it is governed by Newton's law of cooling. No bubble is formed on the heated surface until point (A) Onset of Nucleate boiling is reached at which the first visible bubble is observed. It occurs at low wall superheats ~ 5 ºC. Heat transfer coefficient in this area is the lowest among the other regimes.

1.1.2 Nucleate Boiling Regime

At point (A), the wall superheat is sufficient to activate the first nucleation site. Nucleation sites are small cracks, cavities, pits or crevices that can trap vapor inside. A bubble starts to grow and detach from the surface. The bubble migrates under the buoyancy force to the liquid’s free surface. Both bubble departure from the surface and collapse induce local fluid disturbances that increase heat transfer rate.

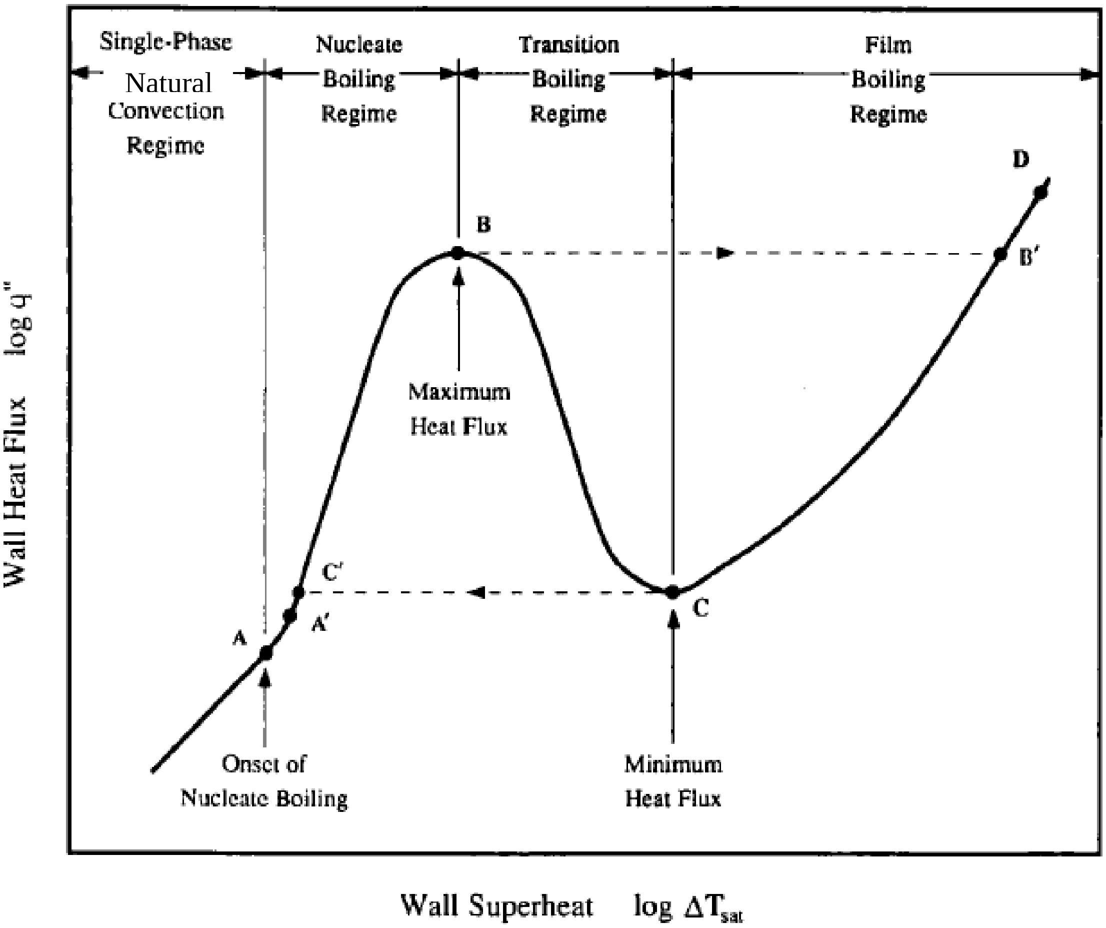

Figure 1.1: The pool boiling curve.

Increasing the wall superheat activates more nucleation sites, increases the rate of bubble formation, and the bubbles get larger such that they coalesce into continuous vapor jets or columns. The fluid flow induced by the bubbles motion and coalesces as well as the high latent heat generation at the surface make the heat transfer coefficient the highest among the different boiling regimes. Ultimately, the heat flux will reach its maximum value at point (B) called Critical Heat Flux (CHF).

1.1.3 Transition Boiling Regime

Increasing the wall superheat beyond the CHF value (using temperature controlled heater) causes the heat flux to decrease. It is due to the formation of vapor film from the continuous bubbles coalesce above the surface acting as an insulating layer. The vapor film coexists with partial nucleate boiling occurring at the surface. The vapor layer increases in size with temperature rise till it covers the whole surface at point (C) which corresponds to the minimum heat flux removed. It is called the minimum film temperature or Leidenfrost point.

CHF represents the limit of operation for power controlled heat transfer applications because any small increase in heat flux will substantially increase the wall superheats from point (B) to point (B') which may exceed the melting temperature of the heated surface material causing burnout of the heater.

1.1.4 Film Boiling Regime

The heated surface is completely covered with stable vapor film at point (C). The heat is currently removed by heat conduction through the vapor film and thermal radiation. The heat flux increases with increasing the wall superheat. The vapor layer gets thicker as the wall superheat increases and the thermal radiation becomes more dominant.

1.2 Nanofluids Methods of Preparation

Nanofluids are produced by dispersing and suspending nanoparticles in a base fluid. These nanoparticles are produced in sizes ranging from 10 to 250 nm. Choi [2] introduced the term nanofluid for the first time in 1995. He reported that the effective thermal conductivity increased by 20% when copper oxide nanoparticles of 10 nm size was dispersed in ethylene glycol. A good nanofluid should have stable suspension and negligible agglomeration of the nanoparticles so they do not drastically alter the nanofluid properties, increase the pumping power or cause clogging. Nanofluids can be prepared using two methods:

1.2.1 The Two-step method

Nanoparticles are first produced as dry powder by physical or chemical synthesis techniques. Then, these nanoparticles are dispersed into a base fluid. Typical physical methods include the inert gas condensation method and the mechanical grinding method. Chemical methods for producing nanoparticles include chemical precipitation, thermal spraying and chemical vapor deposition [3]. The two-step method is widely used in industry as it is more economical. Making nanofluids using the two-step processes is challenging because individual particles tend to quickly agglomerate. This agglomeration is due to attractive van der Waals forces between nanoparticles, and the agglomerated particles tend to quickly settle out of liquids.

Ultrasonic vibrations are used to disperse the particles and reduce its sedimentation. There are other techniques used to enhance the suspension of nanoparticles such as control of acidity (pH) level of the base fluid or addition of surfactants. These contribute to enhance suspension by changing the surface charge of the nanoparticles in which the dissociated ions from the acids or base are attracted to the nanoparticles and overcome the attractive forces of Van der Waals. The two-step method works well for oxide nanoparticles while nanofluids with heavy metallic nanoparticles cannot be prepared with.

1.2.2 The One-step method

The nanoparticles are made and dispersed in base fluid simultaneously. There are several techniques such as single-step direct evaporation (VEROS) and vacuum-SANSS method [4]. These methods are better in preparation of metallic nanofluids. Also, nanoparticle agglomeration is significantly reduced. They exhibit easy control of the nanoparticle sizes and no stabilization techniques are used with this method.

Chapter 2 Literature Review

This chapter presents the previous works that have been carried out on pool boiling of nanofluids. Thermal conductivity of nanofluids is discussed in section 2.1. Studies investigating pool boiling of nanofluids are presented in detail in section 2.2 followed by a brief review of the theory of nucleation in section 2.3. Studies that focused on isolated bubbles generated in a pool boiling system are presented and discussed in section 2.4. The current research objectives and plan are discussed in section 2.5. A description of the thesis structure is provided in section 2.6.

2.1 Thermal Conductivity of Nanofluids

2.1.1 Effect of particle volume fraction

Karthikeyan et al. [5] investigated the thermal conductivity enhancement in two different base fluids of water and ethylene glycol. Only copper oxide nanoparticles of size 8 nm were used in this research. They found that the effective thermal conductivity of the nanofluid increases proportional to the volume fraction of nanoparticles. They reported a 54% increase in the thermal conductivity enhancement with nanofluid volume concentration of 1%. They attributed the thermal conductivity enhancement to the smaller particle size and mono-dispersity of particles. Figure 2.1 shows the ratio of thermal conductivity as a function of the volume fraction of CuO nanofluid.

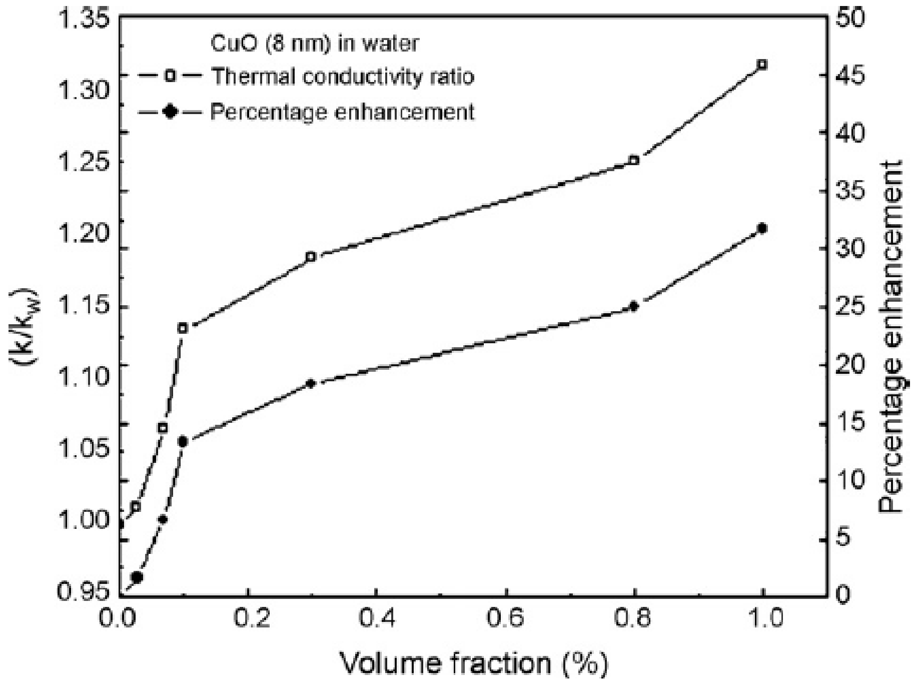

Figure 2.1: The ratio of thermal conductivity and the percentage enhancement of thermal conductivity as a function of the volume concentration of CuO nanofluid [5].

Lie et al. [6] measured the thermal conductivity of alumina water nanofluids of different volumetric concentrations ranging from 0.5% to 6%. The size of nanoparticles used was 47 nm. They found that the nanofluid's thermal conductivity increased with the higher nanoparticles concentration. They reported that the nanoparticles would have stronger Brownian motion and thermophoresis movement. The thermophoresis movement was noticed after the application of heat.

2.1.2 Effect of particle size

Teng et al. [7] studied the effects of several parameters such as nanoparticle size, temperature and concentration on the nanofluids' effective thermal conductivity. They prepared alumina-water nanofluids using three different nanoparticle sizes of 20, 50 and 100 nm. They confirmed the previous results of Lie et al. [6] and Karthikeyan et al. [5] that increasing the concentration of nanofluid increases the thermal conductivity ratio for the same nanoparticle size. In addition, they found that reducing the nanoparticle size increases the thermal conductivity ratio at the same concentration and temperature. By increasing the temperature of nanofluids with different nanoparticle sizes at the same concentration, the thermal conductivity of nanofluid with the smallest particle size will increase much higher than the one with large particle size.

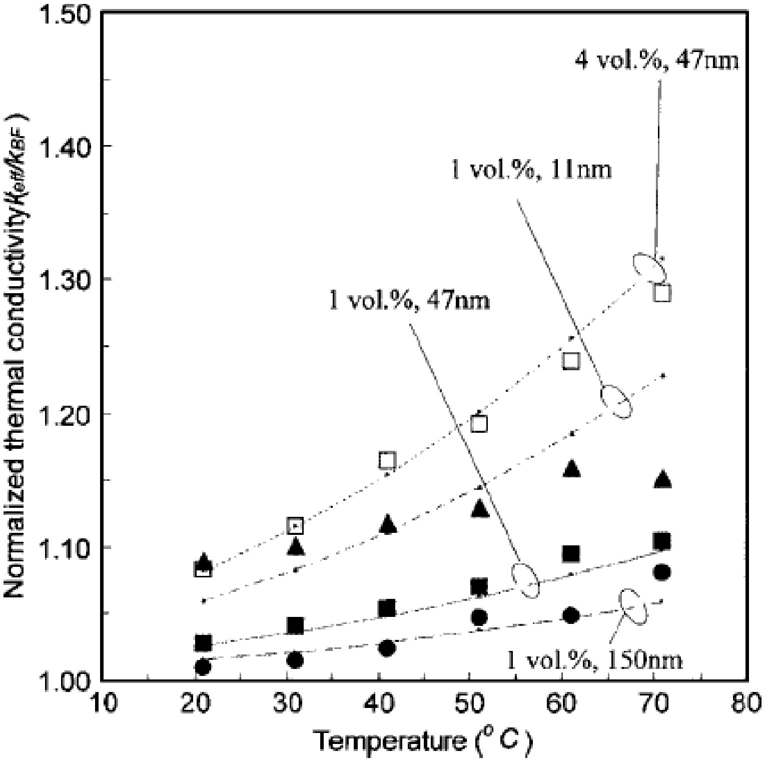

Figure 2.2: The normalized thermal conductivity of Al_2O_3 *nanofluids prepared from different nanoparticle sizes as a function of temperature* [8].

Chon et al. [8] measured the thermal conductivity of Al_2O_3 nanofluid prepared from three different nanoparticle sizes of 11, 47 and 150 nm at 1 and 4 vol. % concentrations. The transient hot wire method was used to measure the thermal conductivity. This method used a thin wire to conduct heat to the liquid for a short period of time before convection starts to take place. The results showed that an increase of the nanofluid thermal conductivity over the deionized water is associated with the decrease in the nanoparticle size used. A maximum thermal conductivity enhancement of 1.15% is reported by using the 11 nm particle. Figure 2.2 compares the thermal conductivity ratios of different particle sizes nanofluids.

2.1.3 Effect of temperature

Teng et al. [7] reported an increase in the thermal conductivity with temperature increase using alumina-water nanofluids with different nanoparticle sizes as mentioned earlier. Mintsa et al. [9] conducted their measurements on two different nanoparticles Al_2O_3 and CuO dispersed into water. They used two nanoparticle sizes for Al_2O_3 (36 and 47 nm) and one nanoparticle size for CuO (29 nm). The transient hot wire method was the measurement technique implemented in this research. Their results showed an increase in the thermal conductivity of both nanoparticles with temperature increase. The same trend has been also reported by Chon et al. [8] as shown in Figure 2.2.

2.1.4 Effect of additives

Surfactants are substances which reduces the surface tension of the liquids when added to it. The structure of surfactants consists of heads (hydrophilic groups) and tails (hydrophobic groups).

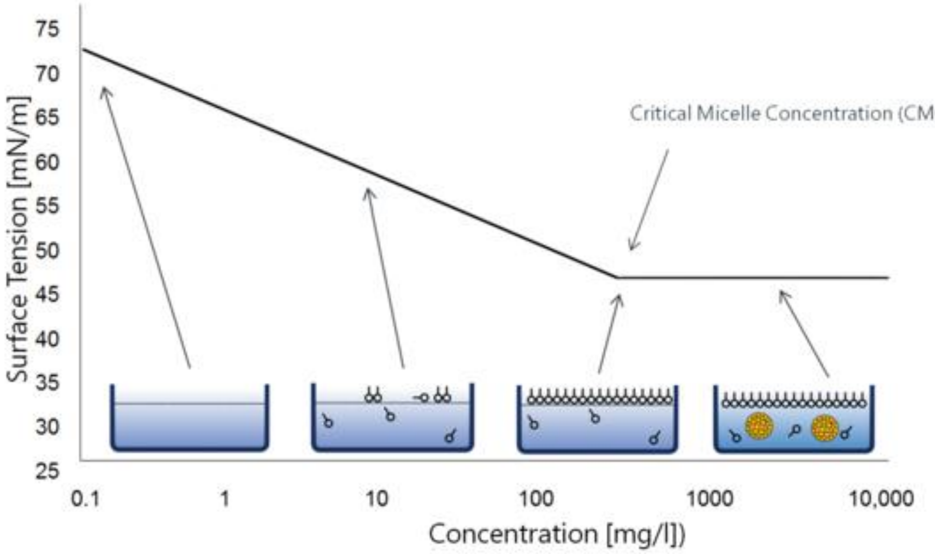

Figure 2.3: Surface tension of a surfactant solution with increasing concentration [10].

When the surfactant is added to liquids at small concentration, it is adsorbed at the free surface of the liquid. The surfactant molecule rearranges itself where its head is in contact with the liquid and the tail extends out of the liquid. This adsorption process is combined with a reduction in the surface tension of the liquid as shown in Figure 2.3. The adsorption process continues with the addition of surfactant till the surfactant concentration reaches Critical Micelle Concentration (CMC). Beyond this concentration, the surface tension reaches its lowest values and the free surface became totally overlaid. Therefore, micelles of the surfactant will start to form inside the bulk of the fluid. The core of the micelles contains the hydrophobic tails and the hydrophilic heads are in contact with the liquid.

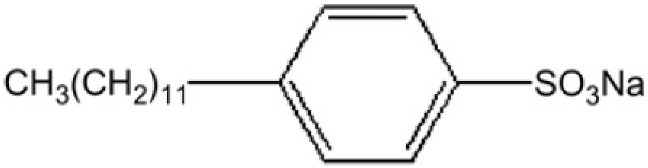

Figure 2.4: Chemical structure of SDBS surfactant [11].

Zhu et al. [11] investigated the influence of dispersants on the stability and thermal conductivity of nanofluids. In this research they used alumina nanoparticles with average size ranging from 15 to 50 nm. The dispersant used was an anionic surfactant, sodium dodecylbenzenesulfonate (referred to as SDBS) in chemical grade. The surfactant structure is shown in Figure 2.4. They prepared different samples of nanofluid with alumina concentration of 0.1 wt. % and different SDBS concentration. The pH value of the samples was maintained at 8.0. The sonication time and frequency were 1 hr and 40 kHz respectively. The measured absorbency and zeta potential values showed similar relationship with SDBS concentration. The absorbency and the absolute value of zeta potential increased with increasing SDBS concentration till a maximum value was reached at 0.10 wt. %. Then they fall down with further increase of SDBS concentration.

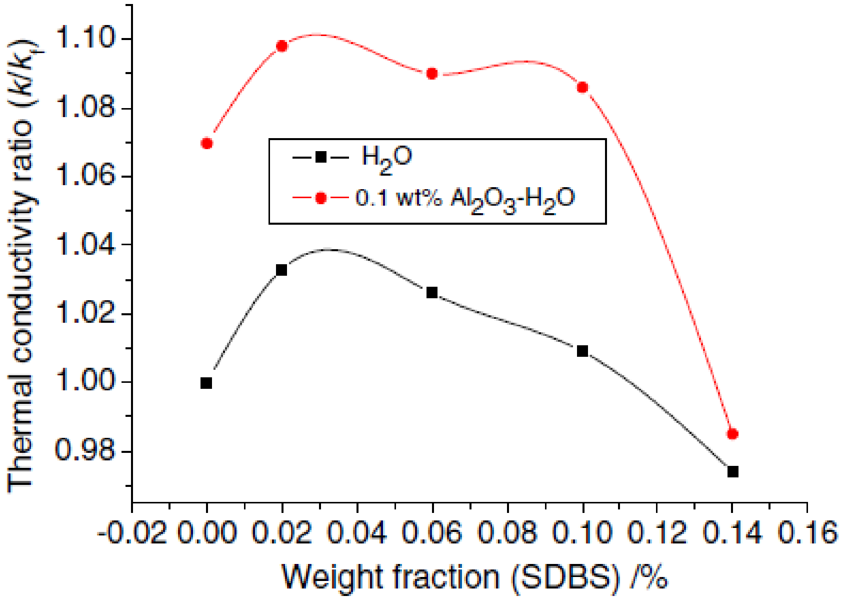

Figure 2.5: The effect of SDBS concentration on the thermal conductivity of alumina nanofluid and water [11].

They illustrated the SDBS dispersion mechanism as follows: Alumina nanoparticles carry positive charge in water. When SDBS is introduced into the suspension, the negatively charged phenyl sulfonic group dissociates and is adsorbed on the alumina surface and consequently the surface is negatively charged. Increasing SDBS concentration pushes the anion groups into the adsorbed layer, and therefore the repulsive forces between the particles is increased that overcome the attractive London-van der Waals forces, increasing the absolute value of zeta potential as well as they will hinder the particles from colliding. When more SDBS exceeds the threshold concentration, Na+ concentration increases. They enter into the absorbed layer reduces the net charge of powder surface and makes the absolute value of zeta potential decrease which means poor nanoparticles suspension.transfere

As surfactants alter the physical properties of the base fluids, thermal conductivity of both the base fluid (water) and the nanofluid were measured against the SDBS concentration as shown in Figure 2.5. The transient plane source (TPS) method was used to measure the thermal conductivity. Both showed similar trend of thermal conductivity. With low surfactant concentration 0.02 wt. %, their thermal conductivities increased quickly. Further increase in concentration to the threshold concentration of 0.1 wt. % caused the thermal conductivities to decrease gradually. Beyond this concentration the thermal conductivities deteriorated very quickly.

2.2 Investigations carried out on pool boiling of nanofluids

Kwark et al. [12] investigated the pool boiling characteristics of low concentration nanofluids. They used different nanoparticle materials: Alumina, copper oxide and diamond. Nanoparticles were dispersed into deionized water at different concentrations (0.001 - 1 g/l) then stabilized and ultrasonicated for two hours. The measured pH values of nanofluids were found far from the IEP point suggesting stable suspensions confirmed with no observation of sedimentation during nanofluid boiling experiments. They measured the thermo-physical properties of the nanofluids and found there was a minimal difference between the properties of nanofluids and that for pure water. Boiling experiments were conducted on a flat copper block attached to electrical heating element.

T-type thermocouple was inserted 1.5 mm away from the surface and was used to estimate the surface temperature. Boiling of Nanofluids with concentrations up to 0.025 g/l showed very similar performance to boiling of pure water, except for critical heat flux (CHF) which increased with increased nanoparticle concentration. 80% CHF enhancement was achieved with 0.025 g/l nanofluids. No information was reported regarding the copper block surface preparation method and roughness.

Heat transfer deteriorations was reported for boiling of nanofluids with concentrations higher than 0.025 g/l as shown in Figure 2.6. The deteriorations in heat transfer increased with the nanofluid concentration. The heat transfer deterioration was accompanied with nanoparticles deposition layer on the heated surface. The layer thickness increased with nanofluid concentration. The decrease in the HTC with increased nanoparticle is regarded to thicker coating created which in turn offers increased thermal resistance. CHF values remained almost the same as that obtained at 0.025 g/l. The different nanoparticle material (copper oxide and diamond) showed a similar boiling performance and CHF enhancement to alumina nanoparticles.

They concluded that nanoparticles material had minimal effect on nanofluid boiling performance. Prolonged boiling experiments were conducted in which several heat fluxes were maintained constant for 120 minutes. Nanofluids exhibited a reduction in HTC with time. In addition, increasing the heat flux imposed was found to increase the magnitude of HTC degradation. However, CHF was reported unchanged.

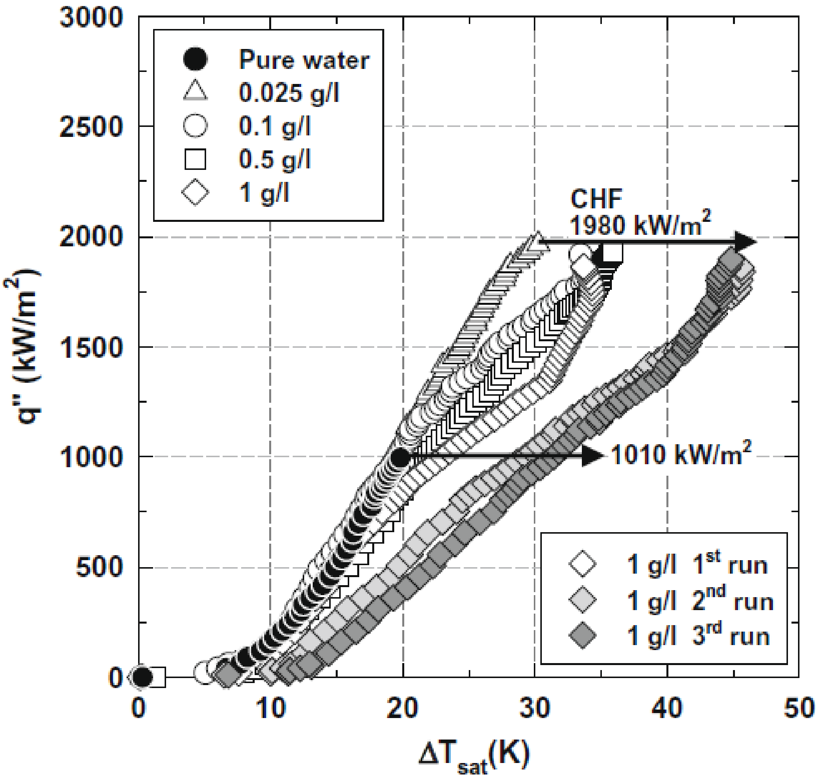

Figure 2.6: Pool boiling curves of nanofluids with concentrations higher than 0.025 g/l [12].

Tang et al. [13] investigated the pool boiling characteristics of δ-alumina/ R141b nanofluids with the addition of surfactants. Nanoparticles of 20 nm size were dispersed into the refrigerant then ultrasonicated for more than 10 hours. Sodium dodecyl benzene sulfonate (SDBS) was added into mixture to enhance the nanofluid stability. Mixtures with different concentrations of nanoparticles and SDBS were boiled over a copper flat surface. The surface was polished with grade 2000 sand paper before each experiment. The surface temperature and heat flux were estimated by four thermocouples that were imbedded along the copper heater axis. The boiling experiments were conducted at atmospheric pressure.

They reported boiling heat transfer enhancement of δ-alumina/ R141b nanofluids at concentrations of 0.001 vol. %, 0.01 vol. % and 0.1 vol. % with addition of SDBS. Boiling heat transfer deterioration was experienced with the 0.1 vol. % nanofluid concentration without any surfactant addition due to the large quantity of deposition of nanoparticles. At very low nanofluid concentration of 0.001 vol. %, the addition of the SDBS decreased the heat transfer enhancement using the nanoparticles. At higher nanofluids concentrations of 0.01 and 0.1 vol. %, the addition of the SDBS increased the nanofluid heat transfer enhancement by improving the nanoparticles suspension and greatly reducing the deposition layer.

In contrast, Chopkar et al. [14] reported boiling heat transfer degradation of water based ZrO_2 nanofluids with the addition of surfactants. Nanofluids were prepared at different volumetric concentrations from 0.005 to 0.15% with ZrO_2 nanoparticle having an average size of 20-25 nm. 1.0 vol. % of tetramethyl ammonium hydroxide (TMAH) were added to some samples of nanofluid as surfactant. The nanofluids were then ultrasonicated for nearly 3-4 hours in order to break the nanoparticles agglomerations. The boiling vessel featured a horizontal copper plate as a heating surface of 60.5 mm diameter. The surface roughness of the plate lies in the range from 0.5 to 0.7 µm. Heat flux is applied to this plate from below by a cylindrical copper heater with four cartridge heaters inserted inside. The plate temperature was measured by T type thermocouple installed 1.5 mm from the plate’s surface.

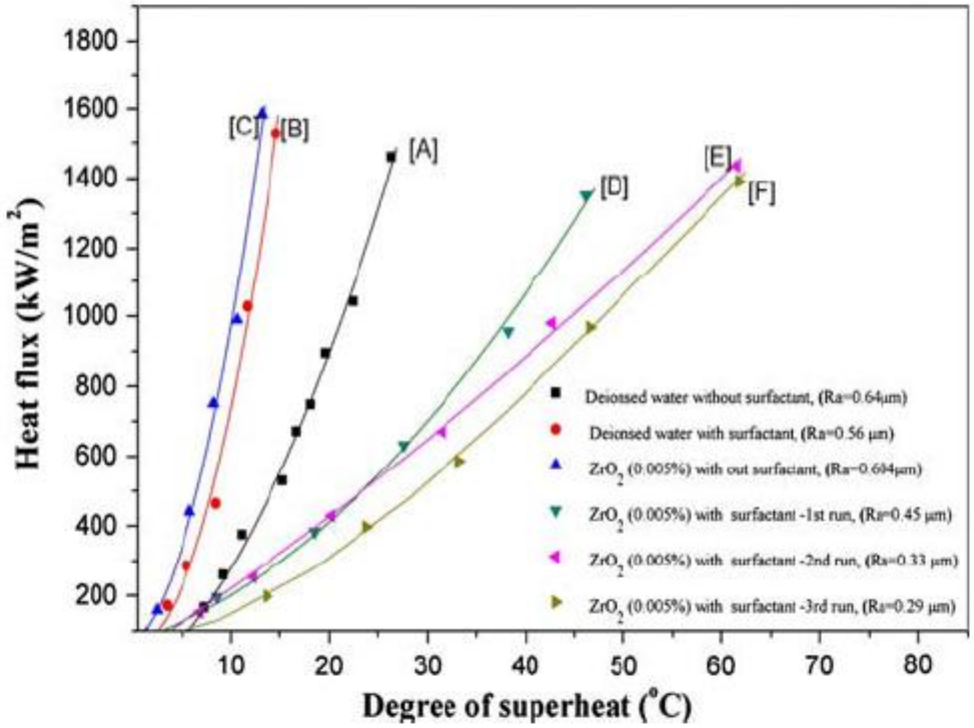

Figure 2.7: Pool boiling curves of deionized water and ZrO_2 *nanofluid with and without surfactant* [14].

They noticed that maximum boiling heat transfer enhancement were associated with the lowest concentration of nanoparticle (0.005 vol. %) (Curve C) and the coefficient of boiling heat transfer in the nucleate boiling region was substantially higher compared to that observed in pure water (Curve A). The increase in nanoparticles concentration had caused a reduction in HTC and the related boiling curve continuously shifted to the right. The only boiling heat transfer deterioration were recorded at nanoparticles concentration of 0.15 vol. %. The boiling performance of 1.0 vol. % aqueous solution of surfactant (Curve B) were examined and found very similar to the performance of 0.005 vol. % nanofluid (Curve C). However, the mixture of both 0.005 vol. % nanoparticles and 1.0

vol. % surfactant (Curve D) deteriorated the boiling heat transfer significantly as shown in Figure 2.7.

Kathiravan et al. [15] conducted pool boiling experiments of Cu/water nanofluids on seamless stainless steel tubes. Different concentrations of nanoparticles were prepared and subjected to vibration in an ultrasonic bath for 10 hours. The actual particle size examined in suspension didn’t exceed 20 nm. The influence of dispersants was included in this research where the boiling heat transfer of nanofluid with and without 9.0% Sodium dodecyl sulfate (SDS) was compared. The heating surface is a horizontal stainless steel tube with an external diameter of 10.6 mm and length of 115 mm. Four thermocouples were located at the inner wall of the tube to measure and estimate the boiling surface temperature. The surface preparation and roughness values were not mentioned.

They concluded a similar relationship between the boiling heat transfer coefficient and nanoparticles concentration to the one found by [14]. They also reported an enhancement in boiling heat transfer by the aqueous solution of surfactant. This enhancement was regarded to an early boiling incipience, small bubble departure diameter and an increase in the number of active nucleation sites. It was observed that irrespective of the presence of surfactants the heat transfer coefficient decreased in the copper-water nanofluid with an increase in the concentration of nanoparticles. Critical heat flux increased with an increase in the nanoparticle concentrations in water and water-surfactant as base fluid. However, surfactant reduced the CHF obtained in the case of water-surfactant nanofluids to one-third of the nanofluids with water as base fluid.

Narayan et al. [16] carried out an experimental investigation of pool boiling of alumina-water nanofluids. They used different nanofluid concentrations ranging from 0.14 to 0.57 vol. %. Alumina nanoparticles used in this research had two different particle sizes of 47 and 150 nm. The pH value of the nanofluid was adjusted to 5.5 to enhance the stability. The heating surface was a vertical stainless steel tube. This new orientation was selected to minimize the effect of sedimentation of nanoparticles on the surface. The heating surface was polished using different emery papers to produce different surface roughness values of 48, 54 and 524 nm.

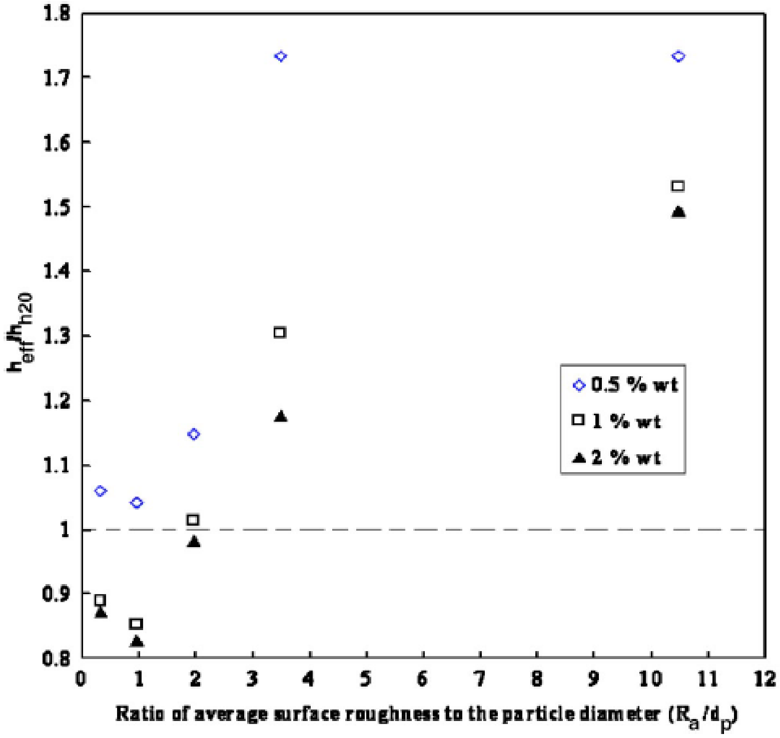

Figure 2.8: The ratio of the nanofluid thermal conductivity as a function of SIP [16].

Their results showed a mix of enhancement and deterioration in heat transfer for different combinations of concentration, surface roughness and particle size. At all concentrations considered in the study, when the particles and surface roughness were of the same order, the heat transfer reached its minimum value. They introduced a new parameter defined as the Surface Interaction Parameter (SIP) which is the ratio of average surface roughness to average particle size. The ratio of nanofluid thermal conductivity as a function of SIP is shown in Figure 2.8. It was noticed that when SIP is unity the heat transfer coefficient is minimum. The HTC is higher when SIP is far from unity. They demonstrated that when particles are smaller than the average surfaceroughness, particles reside within the surface voids causing an increase in the number of active nucleation sites. It was confirmed by taking images of the surface before and after the experiments. Further, they indicated that when SIP is near unity, the nanoparticles block the nucleation sites and deactivate them, which reduce boiling heat transfer.

Wen et al. [17] investigated the effects of heating surface modification on pool boiling of α-alumina/water nanofluids. Nanofluid was prepared at 0.001% nanoparticles concentration and ultrasonicated for two hours. The average size of suspended particles was 405 nm without the addition of any surfactants. Boiling experiments took place on two brass plates having a rectangular shape of 20 X 20 mm^2. The average surface roughness of the plates was 25 and 420 nm.

Comparison between the boiling heat transfer of water and the 0.001% nanofluid on both surfaces revealed that heat transfer enhancement of nanofluid over water was noticed by the smooth surface whereas both fluids exhibited the same boiling performance with the rough surface. Although very low nanoparticles concentration was utilized, nanoparticles deposition layer was found after boiling for both surfaces. For the rough surface, the surface profile did not after nanofluids boiling, with similar peak-to-peak values. However, the averaged roughness of the smooth surface increased over twice for both sampling locations after the first time boiling with nanofluids. The surface modification by nanoparticles was found to be an inherent feature of nanofluids that occurs each time after boiling.

Harish et al. [18] conducted a similar study on the interactions between nanoparticles and heating surface. Alumina nanoparticle with average particle size of 50 nm dispersed in double distilled water was incorporated in this research. Nanoparticles suspension was improved by adjusting the pH value to 4.5. The heating surface is an aluminum disc with a diameter of 20 mm. A lapping machine wet polished the aluminum discs to produce smooth and rough surfaces with average surface roughness of 53 and 308 nm respectively.

Enhancement in the boiling performance was observed in the case of rough heater with the 0.5%, 1% and 2% nanoparticles concentration. However, it was found that the performance of 0.5% and 1% volume concentration nanofluids was nearly same. The smooth heater showed a deteriorated boiling performance and the percentage of deterioration clearly increased with particle concentration. Nanofluid heat transfer deteriorations were reported for the volume concentration of 0.5%, 1% and 2%. They reported that for the smooth heater, the surface-particle interactions decreased the average surface roughness and surface wettability. While for rough heaters, the surface-particle interactions increased the average surface roughness and surface wettability. These effects were found more pronounced at higher nanoparticles concentration and/or wall superheats.

Ahmed, Hamed [19] carried out an extensive research to investigate the effects of various parameters including the nanofluids preparation method, the acidity (pH) and the nanoparticles concentration. They observed that the nanofluid preparation method has a negligible effect on the boiling heat transfer of nanofluids. The decrease in the pH value was found to increase the electrostatic stability of the nanofluids prepared using the two step-method, increase the thermal conductivity of the nanofluids and hence increases the nanofluids' HTC. They reported that the nanoparticles deposition process took place during bubble generation, and release and the rate of nanoparticles' deposition is faster at higher concentrations.

2.3 Theory of Nucleation

Nucleation is the formation process of a vapor bubble within a pool of liquid. Bubble nucleation can be classified into two categories: Homogeneous nucleation and Heterogeneous nucleation. Homogenous nucleation is nucleation happens in the bulk of superheated liquid when there is enough energy to generate a bubble. The nucleation superheat, which is the difference between the liquid and vapor temperatures across the bubble interface, is expressed by Equation 2.1. It describes the minimum superheat required to sustain a bubble of radius (r_{nuc}) where $(dp/dT)_{sat}$ represents the slope of the vapor pressure of the liquid, and it is obtained either from Clausius-Clapeyron equation or the liquid's equation of state.

$$\Delta T_{nuc} = \frac{2\sigma}{r_{nuc}(dp/dT)_{sat}} \qquad 2.1$$

Heterogeneous Nucleation is the process of bubble generation at the solid liquid interface using the vapor entrapped inside its surface cavities. The nucleation superheat required for heterogeneous nucleation is smaller than that for the former case. It can be related to a solid wall by multiplying that for homogeneous nucleation by a factor (φ), Equation 2.2.

$$\varphi = \frac{2 + 2\cos\beta + \cos\beta\,(\sin\beta)^2}{4} \qquad 2.2$$

Since bubbles are usually generated at microcavities with an included angle (θ) on the solid surface, such as that showed in Figure 2.9. The apparent contact angle ($\acute{\beta}$) that will replace β in Equation 2.2 is expressed in Equation 2.3. These equations show that the least nucleation superheat associated with surface cavities. Equations also show that large cavities with large (θ) will nucleate before the cavities with smaller (θ).

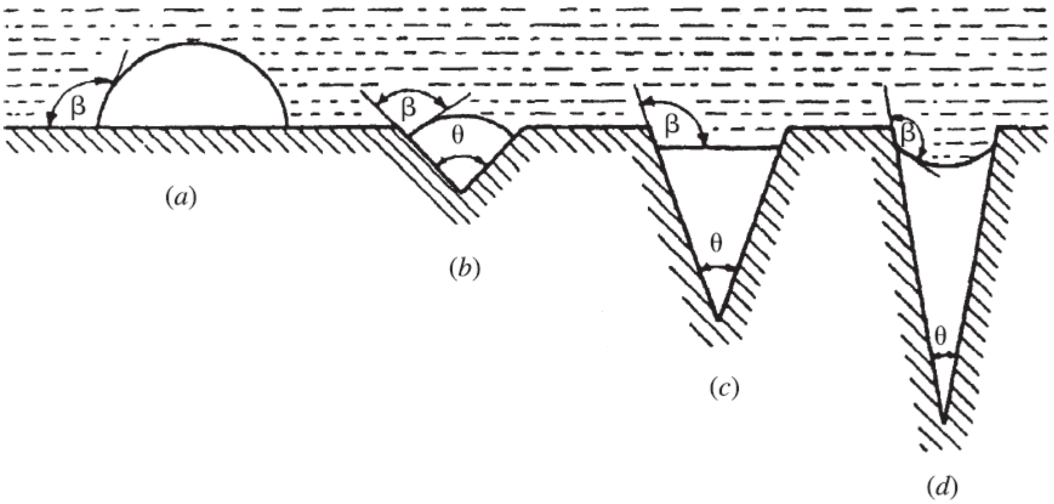

Figure 2.9: Nucleation: (a) plane surface, (b-d) triangular cavity [20].

$$\acute{\beta} = \beta + \frac{\pi - \theta}{2} \qquad 2.3$$

The growth of vapor bubbles is a very complex physical phenomenon. It is influenced by a large number of variables including the surface condition, orientation, the temperature distribution in the bulk fluid and so on. Scientists used simplifying assumptions to help reduce the complexity of the model. They assumed a single spherical bubble growing in a uniformly superheated liquid. Bubble growth consists of two main stages: Inertia controlled growth and heat diffusion controlled growth. In the first stage, the bubble grows very fast by its momentum pushing the surrounding liquid away. Rayleigh [21] modelled the bubble growth through this stage and described the dependency of bubble size on time using Equation 2.4. Then the inertia effects diminish, and the bubble growth enters the second stage in which the bubble continues to grow by the heat transfer from the superheated liquid to the bubble. The bubble growth is much slower than the first stage. Plesset and Zwick [22] derived Equation 2.5 for bubble growth in the heat diffusion stage assuming that the thickness of the thermal boundary layer surrounding the bubble is much smaller than the radius of the bubble.

$$R = \left\{\frac{2}{3}\left[\frac{T_f - T_{sat}(P_f)}{T_{sat}(P_f)}\right]\frac{h_{fg}\rho_g}{\rho_f}\right\}^{\frac{1}{2}} t \qquad 2.4$$

$$R = 2\,C\,Ja\sqrt{\frac{\alpha_f\,t}{\pi}} \qquad 2.5$$

$$Ja = \frac{\rho_f\,c_{pf}\,\Delta T_{sat}(P_f)}{\rho_g\,h_{fg}} \qquad 2.6$$

Where, the constant is $C = \sqrt{3}$ for Plesset and Zwick [22] and $C = \pi/2$ for Forster and Zuber [23]. However, Scriven [24] solved for the bubble growth in the second stage without the assuming thin thermal boundary layer. The same relation given by Plessent and Zwick [22] was obtained for the limiting case of moderate to high superheats. It validates the thin thermal boundary layer assumption for large Jacob number. He also derived a new expression 2.7 which is using for liquids at low superheats or with small Jacob numbers.

$$R = \sqrt{2\,Ja\,\alpha_f\,t} \qquad 2.7$$

Mikic et al. [25] combined the Rayleigh [21] and Plesset-Zwick [22] equations to develop a bubble growth equation valid for the entire bubble growth period. In this model, bubble radius and time are non-dimensionalized; with bubble growth is calculated using Equations from 2.8 to 2.12. At very low of t^+, the Mikic curve approaches the Rayleigh curve, and at very high values of t^+ ,it approaches the Plesset curve.

$$R^+ = \frac{2}{3}\left[(t^+ + 1)^{3/2} - (t^+)^{3/2} - 1\right] \tag{2.8}$$

$$R^+ = \frac{R\,A}{B^2} \tag{2.9}$$

$$t^+ = \frac{t\,A^2}{B^2} \tag{2.10}$$

$$A = \left\{\frac{2\left[T_f - T_{sat}(P_f)\right] h_{fg}\,\rho_g}{3\,\rho_f\,T_{sat}(P_f)}\right\}^{1/2} \tag{2.11}$$

$$B = \left(\frac{12\,\alpha_f}{\pi}\right)^{1/2} Ja \tag{2.12}$$

2.4 Investigations carried out on isolated bubbles in pool boiling

Witharana et al. [26] experimentally investigated the bubble nucleation temperature of individual isolated micro, nanocavities and posts. These features were fabricated on a silicon prime wafer that had very smooth surface with the surface roughness in the sub-nanometer range (Ra ~0.5 nm). The features were fabricated by Electron beam lithography (EBL). The wafer was heated by a 450 W halogen spot lamp mounted above the wafer surface. An infrared camera was used to measure the temperature of the wafer. Great care was taken in the manufacture of cavities on the wafer and degassing of water to ensure that no contaminants or non-condensable gases were present during the experiments.

Figure 2.10 showed that nanocavities with very small mouth diameters as well as posts regardless of their diameters showed very high nucleation temperature close to the nucleation temperature of the wafer with no features at all. They observed bubble generation and departure far away from the feature. The performance of the posts was excepted as they cannot trap any vapor to initiate the nucleation. They also found that increasing the cavity's mouth diameter decreased the boiling nucleation temperature. Their results showed good agreement with the Young-Laplace equation. The authors suggested that low bubble nucleation temperature accompanied with nano-engineered surfaces resulted from the presence of microscale contaminants or surface micro-heterogeneities.

Hutter et al. [27] conducted pool boiling experiments of fluorinert FC-72 at different operating pressure. The heating surface was a silicon chip with isolated artificial nucleation sites. All nucleation sites were cylindrical in shape with a diameter of 10 µm and different depths of 40, 80 and 100 µm. Heat flux was induced to the artificial cavities using thin film resistance heater installed at the back of the silicon chip. Also, microsensors were embedded under the nucleation sites to measure its temperature.

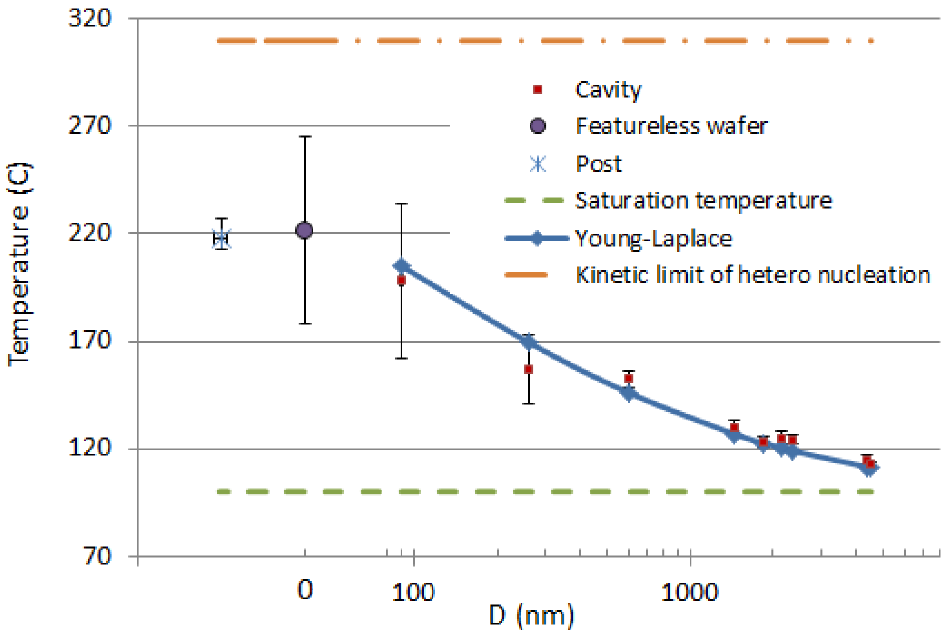

Figure 2.10: The nucleation temperature as a function of the artificial cavity diameter [26].

They observed that bubble frequencies increased with wall superheat increase for the cavities with depths of 80 and 100 µm. For the 40 µm deep cavity, no relation between the bubble frequency and wall superheat was concluded. The operating pressure increase was found to decrease the bubble frequencies for all cavity depths. However, the operating pressure and the depth of cavity had no influence on the bubble departure diameter. Bubble departure diameter increased with the wall superheat increase. Waiting times between bubbles decreased rapidly with increasing wall superheat. Again, there was no visible influence of cavity depth and pressure.

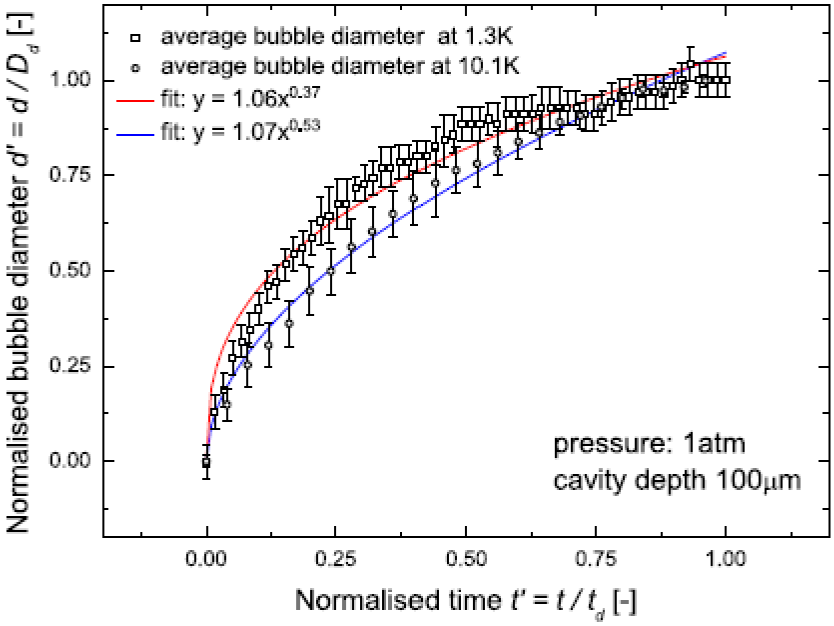

Figure 2.11: The normalized bubble growth rates at different wall superheats [27].

A change in the bubble growth mode was observed by comparison of bubble growth rates at two different wall superheats as presented in Figure 2.11. For the low superheat, the bubble growth rate became very small before lift-off. For the higher wall superheat, the bubble growth rate was higher in the heat diffusion mode, and the bubble departed more suddenly. The equivalent bubble diameter was proportional to time to the power of 0.5 as predicted by Plesset and Zwick [22].

Gerardi et al. [28] investigated the temporal and spatial temperature variations on the heated surface around bubble nucleation sites. In their research, deionized water was boiled on a thin film of Indium-Tin-Oxide (ITO) which was vacuum deposited on a 400 μm sapphire substrate. Heat flux was applied to the surface by conducting electric current through the ITO film. As the ITO film has the property of being opaque in the IR range and the sapphire is transparent to light. IR camera and high-speed video system were installed at the bottom side of the substrate to record the temperature distribution of the ITO film as well as images of the bubble growth on the heated surface.

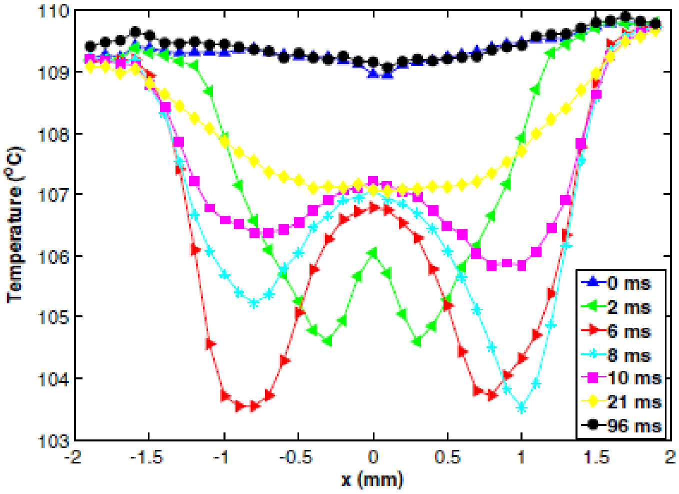

Figure 2.12: Spatial and temporal temperature distribution around a growing bubble [28].

Experimental data acquired from the synchronized systems of HSV and IR camera resolved many details about the bubble growth rates and the mechanisms behind them. The outer bubble radius was observed to increase quickly at first then the rate of radius increase reduced afterwards. Spatial and temporal temperature distribution, shown in Figure 2.12, indicated an abrupt reduction of surface temperature upon the start of nucleation. Comparison of the radius of this cold spot with the outer bubble radius from the HSV system showed very close values and confirmed the initial hemispherical bubble growth. Later, a dry spot was developed centrally inside the cold spot and the outer bubble radius increased significantly over the radius of the cold spot. The temperature and size of the dry spot increased with time. They proved the existence of microlayer evaporation with the IR images. These results had a reasonable agreement with Zhao et al. [29] model for the radius of the dry out area and Cooper and Lloyd [30] model of microlayer growth.

Siedel et al. [31] studied the bubbles generation from a horizontal copper plate submerged in a pool of n-pentane at atmospheric pressure. The copper plate was circular with 18 mm diameter and 40 µm thickness. An artificial nucleation site was made by mechanical indentation. The nucleation site had a paraboloid shape. The mouth diameter and the depth of the nucleation site are 180 µm and 500 µm respectively. Heat flux was applied to the plate by a copper pin soldered to it. They found that the shape of the evolving bubble was not spherical. The bubble departure volume remained unchanged with the increase of wall superheat whereas the bubble growth time decreased significantly. The normalized bubble volume at different wall superheats was proportional to the normalized time to the power of 0.6.

2.5 Research Objectives and Research Plan

Although the pool boiling of nanofluids has been extensively studied for many years, contradicting results of boiling heat transfer enhancement and deterioration were reported by several researchers. The objective of this study is to investigate parameters that are suspected to explain the contrary findings in the literature, and gain a better understanding of pool boiling of nanofluids. The first parameter that has been investigated is the heated surface condition. Several researchers explained the different boiling characteristics of nanofluids as a result of various nanoparticles interactions with the surface textures and cavities. Also, the randomness of the surface texture added complexity to the boiling phenomenon. The second parameter that has been considered is nanoparticles stability. Nanofluids prepared from dry nanoparticles exhibited poor stability. The particles easily agglomerate in clusters that deposit on the heated surface and hence reduce the rate of heat transfer due to the added heat resistance. The effect of the use of surfactants on nanoparticles deposition has also been investigated.

The current experiments have been carried out in three stages:

- Stage 1: A set of experiments have been carried out to investigate the effects of the heated surface roughness.
- Stage 2: A set of experiments have been carried out to investigate the effects of nanoparticles concentration and surfactant concentration.
- Stage 3: A set of experiments have been carried out to investigate the isolated bubbles formation and bubbles growth rates, in both pure water and nanofluids.

In this study, Alumina Oxide Al_2O_3 nanoparticles suspended in deionized water were used. Al_2O_3 has been commonly used by other researchers and used here for results comparison. Sodium dodecylbenzenesulfonate (SDBS) was used as a surfactant. The boiling surface was made from copper. Unlike conventional surface preparation techniques used in the literature, a diamond turning machine was used to produce the boiling surface.

2.6 Thesis Structure

Chapter 3 provides details of the experimental facility, methodology and validation of the experimental setup. Chapter 4 presents experimental results obtained for the three stages mentioned before. Chapter 5 includes the summary and main conclusions. Recommendations for future work are presented in Chapter 6.

Chapter 3 Experimental Setup and Methodology

This chapter provides detailed information about the experimental setup and the analysis used in this research. The details and components of the experimental setup are described in section 3.1. The calculation of the applied heat flux and the surface temperature are discussed in section 3.2. Section 3.3 reports the uncertainty analysis of the experiments data. The parameters investigated throughout this research are introduced in section 3.4. Nanofluid preparation method and the boiling surface preparation are discussed in sections 3.5 and 3.6 respectively. Details of the test rig operation procedure are presented in section 3.7. Sections 3.8 and 3.9 provide insight information regarding the validation and repeatability of the experimental results.

3.1 Experimental Setup

The boiling vessel used in this experimental investigation is shown in Figure 3.1. It is constructed from stainless steel pipe (13) with a diameter of 20 cm. This vessel is divided into two sections by a stainless steel skirt (16) that is installed inside the pipe to contain the working fluid inside the pipe and hold the boiling surface horizontally in place. At the upper section of the vessel where the liquid is contained. Two heaters, which are called Bulk Fluid Heaters (4), with a rated power of 3000 W, are wrapped around the outside perimeter of the pipe. These heaters serve to control and maintain the temperature of the bulk fluid temperature at a prescribed value. This is achieved by connecting one 3.2

mm diameter type-E thermocouple immersed in the bulk fluid to Watlow PID controller. The heaters are connected to the PID controller through an ON/OFF solid-state relays. The PID controller will achieve the pre-defined bulk fluid temperature through estimating the heaters ON mode duration required to change the fluid temperature from the actual value measured by the thermocouple to the pre-defined one. When the temperature reaches this value, the controller will turn off the heaters. Another two similar thermocouples are installed and connected to the data acquisition system to record the bulk fluid temperature.

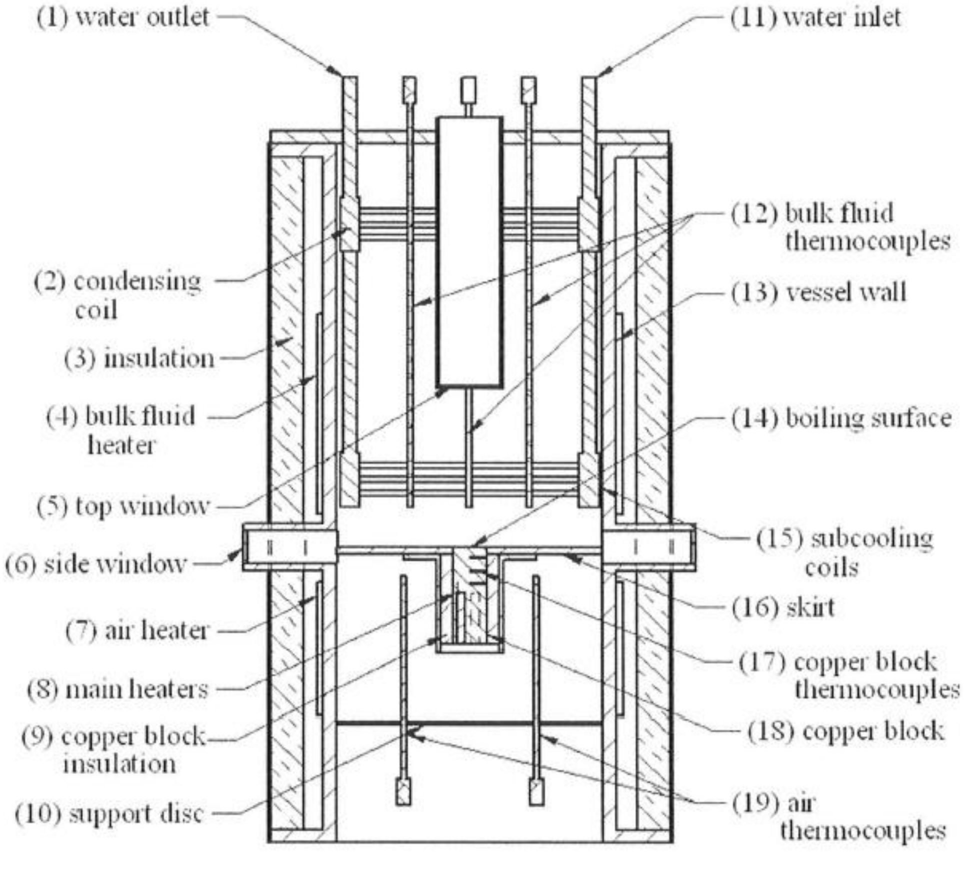

Figure 3.1: The boiling vessel.

At the lower section of the vessel, there is a third band heater, which is referred to as Air Heater (7), wrapped around the vessel. This heater is used to raise the air temperature close to the temperature of the system. This serves two purposes: reducing the heat loses of the bulk fluid through the stainless steel skirt and minimizing the heat loses from the boiling surface heating element. A support disc (10) is installed at the bottom end of the pipe to confine the air inside the pipe and prevent the air mixture with the air in the room. The control of the air heater is made in a similar fashion to the bulk fluid heaters using one thermocouple installed in between the skirt and the support disc. Another thermocouple is installed at the same location to record the air temperature through the data acquisition system.

A condensing coil (2) is used to maintain a constant amount of the liquid during the experiment. This feature is very important for the pool boiling experiment of nanofluids. It will help maintain the same concentration of nanofluid during the experiments. The condensing coil water flow rate is controlled and monitored by a needle valve and a flow meter. The water temperature entering the coil is controlled by a water heater installed in the water system before the condensing coil. This heater helps to adjust the condensing coil temperature to prevent the bulk fluid from subcooling. The condensing coil's water flow rate and temperature have been selected after three test runs to ensure no loss of the base fluid and no change of the nanofluid concentration during the experiments. The condensing coil temperature is recorded by one thermocouple. A drainage/subcooling coil (15) is used to cool down the bulk fluid temperature as a part of the post-experiment procedure. Two opposing glass side windows (6) allow visual observation of the boiling phenomenon on the surface from the side. The diameters of the side windows are 2.5 cm. The whole vessel is wrapped with an aluminum cover to protect the user from contacting the heaters. Insulation (3) is inserted between the cover and the vessel to reduce heat losses from the vessel and conserve power.

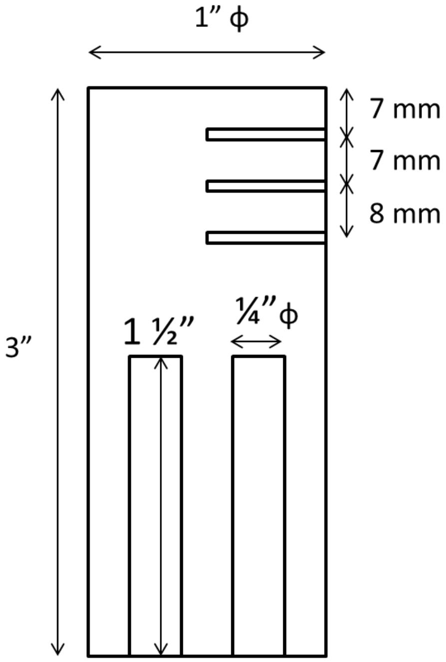

Figure 3.2: Schematic drawing of the copper block of the first boiling configuration showing its dimensions and the locations of the thermocouples embedded in.

In order to conduct the different stages of the experimental investigation mentioned in Chapter two, two different heated surface configurations were designed and implemented. In the first configuration, which is used in Stages 1 and 2 of the experiments, a copper block (18) with a 2.54 mm diameter and 76.2 mm length was installed at the center of the skirt and its top circular surface served as the boiling surface. Three 0.25 inch diameter and 1 inch length cartridge heaters were fixed at the bottom of the copper block to provide the heat flux to the heated surface, referred to as the Main Heaters (8). The maximum power of the main heaters was 750 W, which was capable of providing a maximum heat flux of 1.48 kW/m^2. The axial temperature profile of the copper block has determined using three 1.0 mm diameter type-E thermocouples (17) installed at different axial distances from the top of the block. The locations of the thermocouples in the copper block are shown in Figure 3.2. The copper block was wrapped in a sheet of Fiberfrax insulation (9) to reduce radial heat losses.

In the second configuration, which was used in Stage 3 of the experiments, a flat sheet of copper (20) with a thickness of 1 mm was attached to the top surface of the skirt (16) and a cone-shaped heating element (21) made from copper touched the back or the dry side of the sheet in a very small area. The cone heating element was connected to a precise threading mechanism (22) that controlled its axial location. In this configuration, there was only one heater of 250 W used. The surface temperature of the sheet was measured by using a self-adhesive, fast response type-E thermocouple. The whole mechanism was insulated with Teflon (23) to minimize heat losses. Figure 3.3 and Figure 3.4 depict the details of the second configuration.

All experiments carried out in the present study for both configurations are, pool boiling power-controlled experiments. Therefore, the PID controller was adjusted to control the electrical power input to main heater.

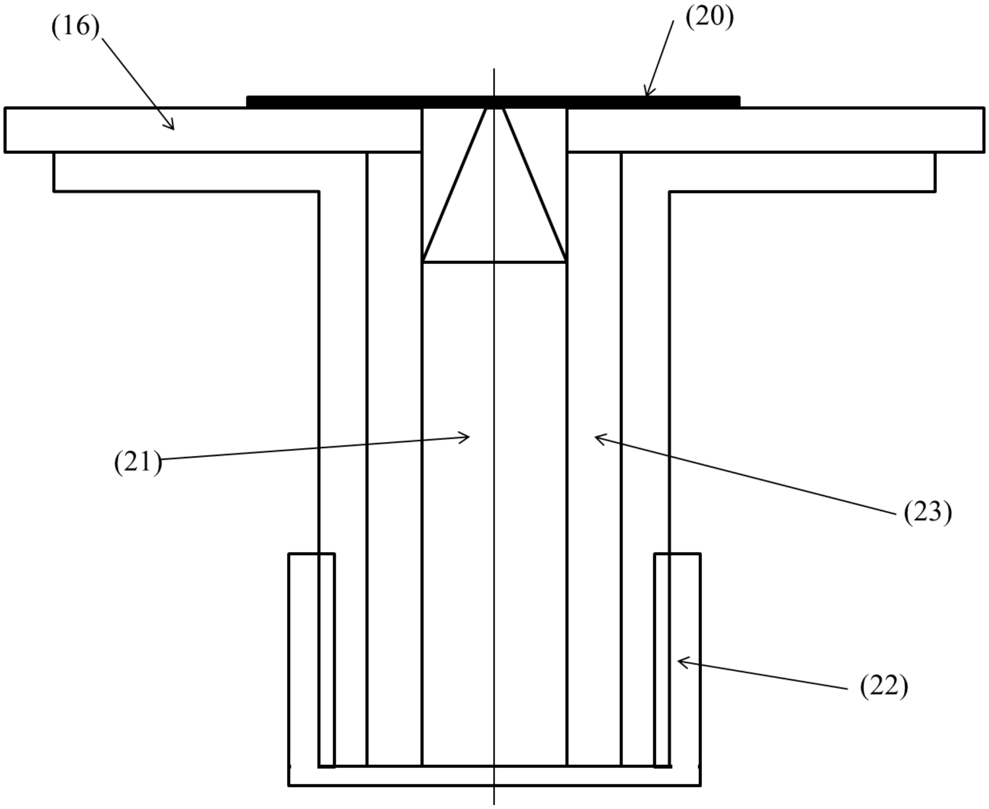

Figure 3.3: Schematic drawing of the second boiling configuration.

All temperatures measured by the thermocouples were acquired using a PC using a Kiethley Data Acquisition System Model 2700. The electrical signal data sent by the thermocouples were decoded using an ExceLinx software installed in Microsoft Excel. The software converts the signals into the equivalent temperature values. The data sampling rate was 0.2 samples per second. All thermocouples were calibrated using a Resistance Temperature Detector (RTD) which was calibrated to 0.01 ºC. The calibration was carried using an insulated oil bath surrounded by an electric heater. The oil bath temperature was raised using a PID controller of the heater until the temperature of the

RTD reached steady-state. It was assumed that the temperature was uniform in the oil bath. The RTD and thermocouples temperatures were recorded using the same wires and same data acquisition system used in the actual experiments to account for the deviation in the readings from the wiring and connections. A linear best fit was used to correlate the thermocouple readings to the RTD. To check that the fit was accurate, the R^2 values were calculated and were found to be 0.999.

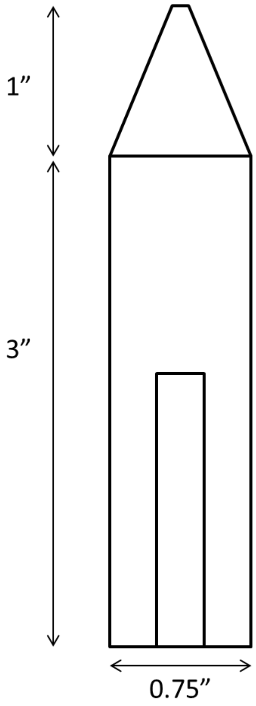

Figure 3.4: Drawing of the heating element in the second boiling configuration.

High-speed images of the water and nanofluid boiling experiments were recorded using Photron FASTCAM 1024PCI high-speed imaging camera. A Lower Pro light source was used to provide the illumination for the camera. The camera was placed at one of the side windows, and the light source was placed at the other side window. The adjustment of the lens aperture and the brightness of the light source were critical to distinguish the growing bubbles from the background in high opaque fluids and ensure good image quality. The images were recorded at a rate of 3000 frames per second. The resolution used was to 640 x 480 pixels, which was found to be adequate to observe the bubbles clearly.

3.2 Calculation of the applied Heat Flux (q'') and the Surface Temperature (T_s)

The temperature profile of the heating element, which was developed by three thermocouples installed at different axial distances from the boiling surface was used to estimate the heat flux applied to the boiling surface. The heat transfer model inside the heating element was assumed as one-dimensional heat conduction without heat losses from the side. Therefore, the measured temperatures were fitted to a linear temperature profile and the heat flux applied was estimated from Equations 3.1.

$$q'' = k\, \frac{n \sum x_i T_i - \sum x_i \sum T_i}{n \sum x_i^2 - (\sum x_i)^2} \tag{3.1}$$

$$T_s = \frac{\sum T_i \sum x_i^2 - \sum T_i x_i \sum x_i}{n \sum x_i^2 - \left(\sum x_i\right)^2} \tag{3.2}$$

Where: n = number of temperature readings, i = ith reading.

The locations of the thermocouples in the heating element used in the first heated surface configuration are shown in Figure 3.2.

For the surface temperature of the first boiling configuration, the linear fit temperature profile is extrapolated, and the surface temperature is estimated from equation 3.2. Whereas in the second boiling configuration, the surface temperature is directly measured using self-adhesive, fast response thermocouples assuming that there is no temperature gradient across the sheet thickness.

The wear in the copper block used in the first boiling configuration due to re-machining of the surface was quantified by measuring the overall height of the copper block using a Vernier caliper before every experiment. The reduction in the height of the copper block was calculated for each experiment and subtracted from the distances of the thermocouples from the copper block surface.

3.3 Uncertainty Analysis

The uncertainty analysis was carried out according to Equation 3.3.

$$u(R) = \sqrt{\left[\left(u(W_1)\frac{\partial R}{\partial W_1}\right)^2 + \left(u(W_2)\frac{\partial R}{\partial W_2}\right)^2 + \cdots + \left(u(W_n)\frac{\partial R}{\partial W_n}\right)^2\right]} \qquad 3.3$$

Where: $u(\ldots)$ = uncertainty in $(\ldots)$, R = calculated result, and W_n = nth variable.

3.3.1 Uncertainty in Measured Temperatures

The uncertainty in the temperatures recorded was ±1.7 °C as provided by the thermocouples supplier. The thermocouples were 1.0 mm in diameter, and the holes drilled in the copper block were 1.1 mm diameter. It gives an uncertainty in the thermocouple location of ±0.05 mm.

3.3.2 Uncertainty in Heat Flux (q'')

The uncertainty in the applied heat flux is due to the uncertainty in the temperature gradient in the heating element. Calculating the uncertainty in q'' using Equation 3.3 gives a maximum experimental uncertainty of ±59.7 KW/m2. The intermediate applied heat flux was 500 KW/m^2, respectively. Therefore, the uncertainty in the heat flux was 12 %.

3.3.3 Uncertainty in Surface Temperature (T_s)

The uncertainty in surface temperature was calculated using Equation 3.3, which yields an uncertainty in the surface temperature of ± 2.4 °C for the first boiling configuration, and ± 1.7 °C for the second boiling configuration. Using an intermediate surface temperature of 118 and 105.94 °C, the uncertainties in surface temperature are 2.0 % and 1.6 %, respectively.

3.3.4 Uncertainty in Bulk Fluid Temperature (***T_{sat}***)

The bulk fluid temperature was recorded using two thermocouples. The average of the two temperatures was calculated and used as the saturation temperature, as shown in Equation 3.4.

$$T_{sat} = \frac{T_1 + T_2}{2} \tag{3.4}$$

The error in each thermocouple was ±0.5 °C each, which yields a combined error of ±0.35 °C in the liquid saturation temperature. For an average liquid saturation temperature of 100 °C, the uncertainty in bulk fluid temperature is 0.35 %.

3.3.5 Uncertainty in Surface Superheat (***T_s - T_{sat}***)

The uncertainty in surface superheat is due to the uncertainty in surface temperature and liquid saturation temperature. Combining the two using Equation 3.3 gives an uncertainty in surface superheat of ± 2.42 °C for the first boiling configuration, and ± 1.73 °C for the second boiling configuration.

3.4 Parameters Investigated and Conditions of the Experiments

3.4.1 Stage 1: Effects of the heated surface roughness

It was suspected that the heated surface texture and surface roughness has a significant influence on the nanofluids boiling phenomenon. As indicated before past research [16]–[18] showed contradicting results regarding the interaction between the nanofluids and the heated surface texture. The nanofluids preparation method used in stage 1, which is discussed in detail in section 3.5, is based on the findings reported in [11], [32], [33] which recommended the use of dispersants to increase the nanoparticles suspension and improve the stability. The nanoparticles mass concentration was kept constant at 0.05 wt. % during this stage, as this value was one of the most commonly used in the literature and permits comparison to other research.

The effects of the heated surface roughness were investigated at this stage of the research. Nanofluid preparation method in [11], [32] is adopted and tested against a rough and smooth heated surfaces. The first heated surface configuration was utilized in this stage of experiments. Two boiling surfaces with average surface roughness of 6 and 60 nm were produced by using diamond turning machine. The surface roughness was measured at five different locations on the boiling surface before each experiment to determine the average surface roughness. The locations of surface roughness measurements are shown in Figure 3.5.

3.4.2 Stage 2: Effects of nanoparticles concentration and surfactant concentration

In this stage, two nanoparticles concentrations of 0.05 and 0.1 wt. % were tested using the smooth surface (Ra = 6 nm). No surfactant was added to the nanofluid to investigate the nanoparticles and the heated surface interactions.

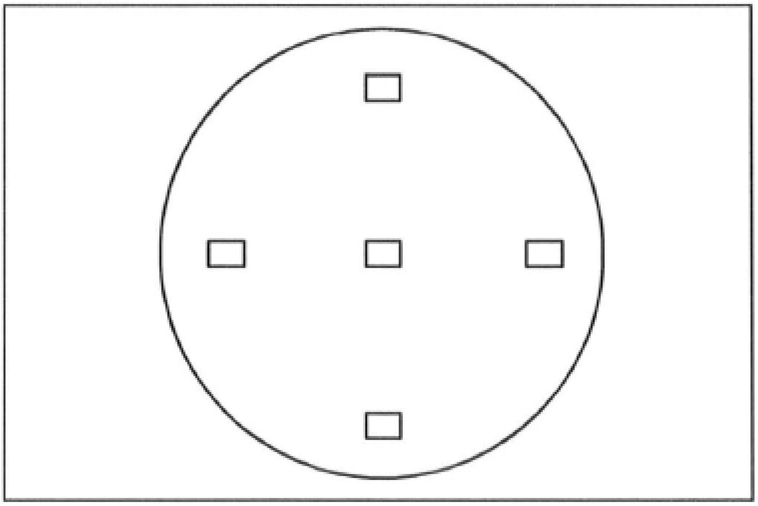

Figure 3.5: Locations of the surface roughness measurements of the first heated surface configuration.

Another set of experiments was conducted using the rough surface (Ra = 60 nm) investigating the effect of the surfactant concentration. Two concentrations of 0.1 and 1.0 wt. % were considered. The nanoparticles concentration during these experiments was maintained at 0.05 wt. %. The first heated surface configuration was utilized in this stage. The heated surface was prepared similar to stage 1.

3.4.3 Stage 3: Investigation of isolated bubbles formation and bubbles growth rates

The nanoparticles interaction with a single nucleation cavity was investigated experimentally using the second heated surface configuration. The second configuration was designed and built to provide a small local area of the surface with heat flux necessary to nucleate single isolated bubbles. Pool boiling experiments of deionized water were conducted first followed by boiling experiments of the nanofluid. The nanofluids concentration was kept constant at 0.05 wt. %. The SDBS surfactant was not used in order not to alter the thermo-physical properties of the nanofluids using the surfactant. Unlike the first two stages of the experiments, the boiling surface was prepared using sand papers. The average surface roughness was measured and found to be 120 nm.

3.5 The Nanofluids Preparation

The nanofluids preparation method used in this experimental study is a two-step method. This method is widely used in the literature, and it allows for comparison with other experimental data. In this two-step method, dry powder of nanoparticles which is produced by the chemical or physical method is dispersed and suspended in the base fluid. Alumina (Al_2O_3) nanoparticles were acquired in dry form from Nanophase Technologies Incorporation. A nominal particle size of 10 nm is reported by the manufacturer. Deionized water is the base fluid in this study. Surfactants are also incorporated in the preparation of nanofluid for its good dispersion characteristics [11], [32]. Sodium dodecylbenzenesulfonate (referred to as SDBS) is an anionic surfactant in a chemical grade provided by Sigma Aldrich was used.

Because of the health hazards associated with inhaling the nanoparticles dust during the weighing and dispersing processes, the complete preparation process is conducted in a fume hood. Amounts of alumina nanoparticles, as well as SDBS surfactant, are carefully weighed and dispersed in deionized water. After stirring the mixture, the nanofluid is ultrasonicated for 30 minutes in an ultrasonic bath with a frequency of 40 kHz. The ultrasonic vibration was used to break down particle agglomerates as nanoparticles have a high tendency to agglomerate due to strong Van der Waals forces [4]. This duration has been selected based on the work of Yousefi et al. [33] to find the necessary sonication time. As different researchers used either the volumetric or weight concentration to express the nanofluid composition, Equation 3.5 is used to switch between the different systems [15].

$$\emptyset_v = \frac{1}{\left(\frac{1-\emptyset_m}{\emptyset_m}\right) \times \frac{\rho_{np}}{\rho_f} + 1} \tag{3.5}$$

After the nanofluid preparation is completed, a sample of it is analyzed by the Dynamic Light Scattering (DLS). This machine measures the nanoparticles size profile in suspension using a projected laser on the nanofluid sample. Due to the Brownian motion of the particles, the laser scattering constantly changes. The laser intensity is found to change depending on the size of particles in suspension as shown in Figure 3.6. The intensity is fed to a correlation that gives the range of the particles size in suspension.

.

3.6 Heated Surface Preparation

Due to the interactions between nanoparticles and the heated surface, the formation of deposition layer in nanofluids boiling experiments as well as aged or oxidized surfaces give different boiling characteristics; the boiling surface was prepared each time an experiment took place. Common surface preparation techniques that had been used in the literature included sandpaper polishing and electric discharge machining

(EDM). These methods produced random surface texture in which size of active nucleation sites varies greatly, and the nucleation site density is not consistent over the boiling surface.

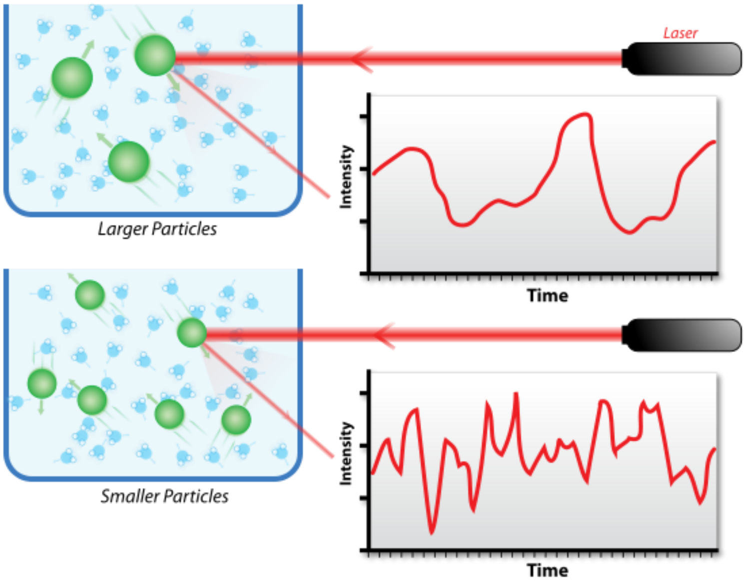

Figure 3.6: The dependency of the laser intensity on the size of the suspended particles [34].

A diamond turning machine is incorporated to produce the boiling surfaces in Stages 1 and 2 of experiments. This machine offers very rigid structure that eliminate tool cutting vibrations, precise cutting tool feeding drives in the micrometers scale and diamond tipped tools that exhibit very high strength and wear resistance. The machined surfaces have a mirror surface finish possess consistent surface texture. The peaks and valleys are equally distributed across the surface. Figure 3.7 depicts the different heated surface texture generated by hand polishing and diamond turning machining.

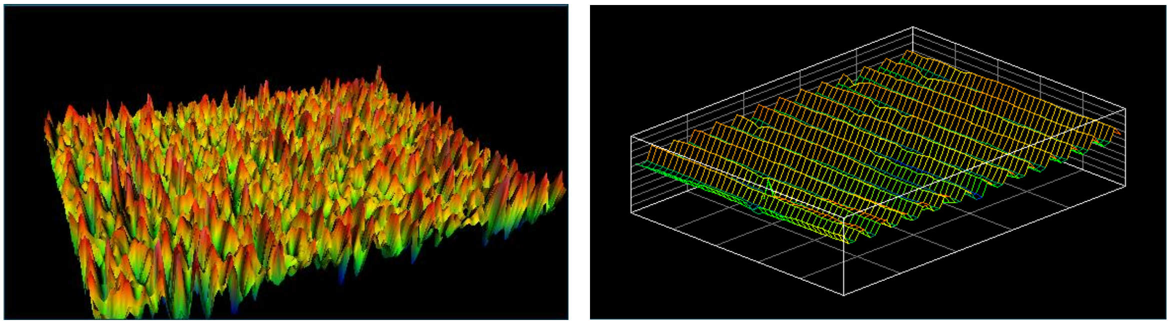

(a) *(b)*

Figure 3.7: The heated surface texture generated by: (a) Sand polishing, (b) Diamond turning machine.

In Stage 3 of experiments, the diamond turning machine was broken down. Therefore, the surface preparation of the flat copper sheet is done by sand polishing. Different grades of sand paper were used. The polishing process was done in two perpendicular directions and water was used as a lubricant. This procedure helped to reduce the deviation of the surface roughness readings. The average surface roughness was 120 nm.

3.7 Test Procedure

The experimental test procedure begins with complete washing and cleaning to all parts of the boiling vessel from the residual nanofluid that may exist. Then the boiling vessel assembly took place. Flange management is applied to the stainless steel skirt to prevent leakage. Main heaters and thermocouples are installed in their locations. Thermal paste is added to empty the voids from the air and reduce the thermocouple temperature fluctuations. Also, it reduces the contact resistance at the heaters. The working fluid is added to the boiling vessel. The vessel usually contains 5 liters of liquid. Both the bulk fluid and the air heaters are turned on after the insulating cover is installed. The bulk fluid heater is in automatic control mode with a temperature setting of 104 °C. The same settings apply to the air heater except that the temperature setting is 110 °C. The controllers were set to a slightly higher temperature than the required because the final temperature of the liquid or air was found to be always a few degrees lower than the set temperature on the controller. When the fluid temperature reaches the saturation temperature, the control mode of the bulk heater is switched to the manual mode with 50 % power setting for 15 minutes with the inlet condensing water flowing at a rate of 200 cm^3/min. The inlet condensing heater is also switched on. The inlet condensing water temperature should reach a temperature of 50 °C. At this point, rigorous boiling of the fluid causes the non-condensable gasses to evaporate. After the 15 minutes have passed the bulk fluid heater is switched back to the automatic mode. The main heaters are switched on. The power percentage is set and controlled by the PID controller. Steady state temperature profiles are achieved after a nominal period of 2 minutes. The steady state is recognized by the thermocouples temperature changes not higher than 0.1°C over a period of 30 seconds. After the steady state is achieved, all temperatures are recorded, and the main heaters power is increased and this procedure is repeated.

3.8 Validation of Water Boiling Curve

The results of the experimental setup have been validated by conducting pure water boiling experiment on the smooth surface with an average roughness of 6 nm. The water boiling curve has been compared to the Rohsenow correlation. The constants of the correlation used are $s = 1$, $r = 0.33$ and $C_{sf} = 0.0128$. The pool boiling curve shows very good agreement with the correlation as presented in Figure 3.8.

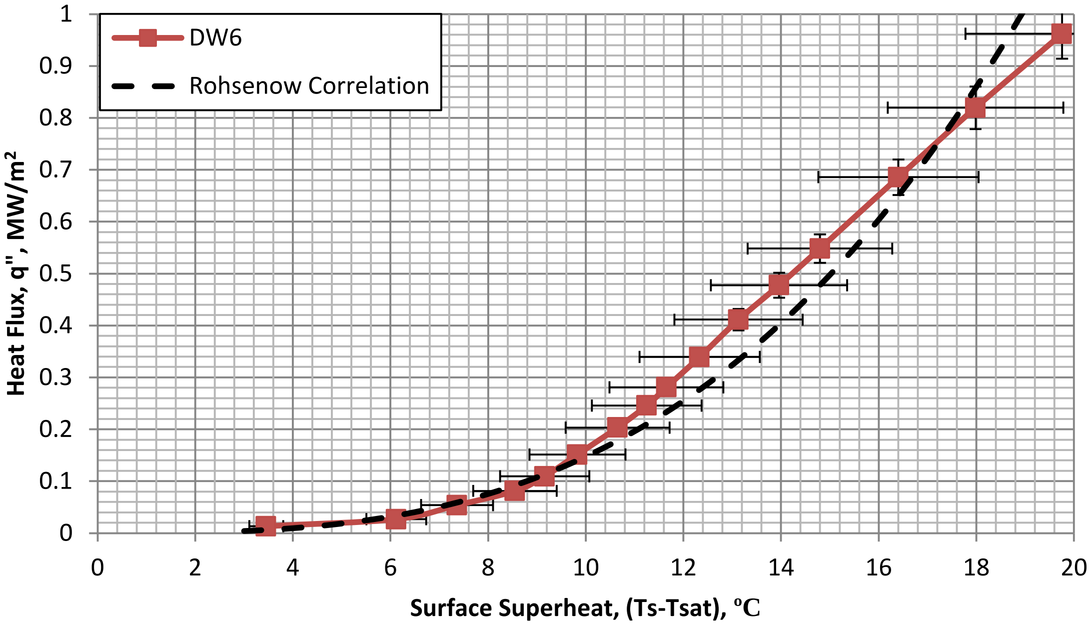

Figure 3.8: Water pool boiling curve compared against the Rohsenow correlation.

3.9 Experiments Repeatability

The repeatability of the various boiling curves has been examined by repeating three different boiling experiments from Stage 1 and 2 experiments. The experiments were: pure water experiment on the smooth boiling surface, nanofluid with nanoparticles concentration of 0.05 wt. % and surfactant concentration of 0.1 wt. % on the smooth boiling surface and surfactant aqueous water with a concentration of 1.0 wt. % on the rough boiling surface. These experiments were selected to ensure not only the accuracy of the boiling vessel but also to confirm the precision of the surface preparation as well as the nanofluid preparation. Results of the experiments are shown in Figures Figure 3.9 to Figure 3.11. All boiling curves lie within the experimental error showing good agreement is established.

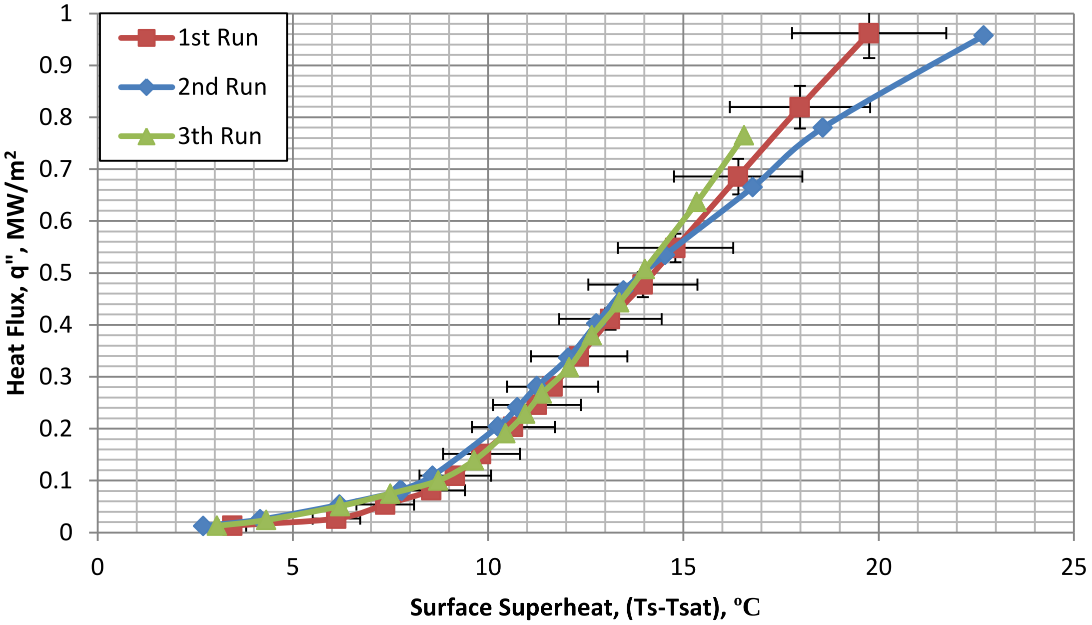

Figure 3.9: Repeatability of pure water boiling curves on the smooth boiling surface.

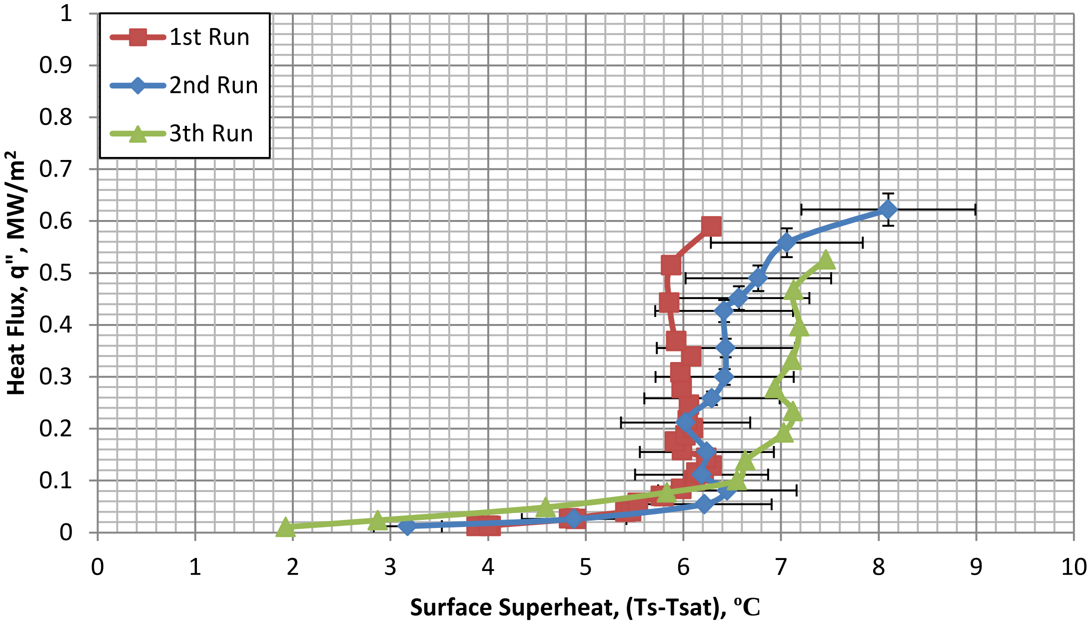

Figure 3.10: Repeatability of nanofluid boiling curves on the smooth boiling surface.

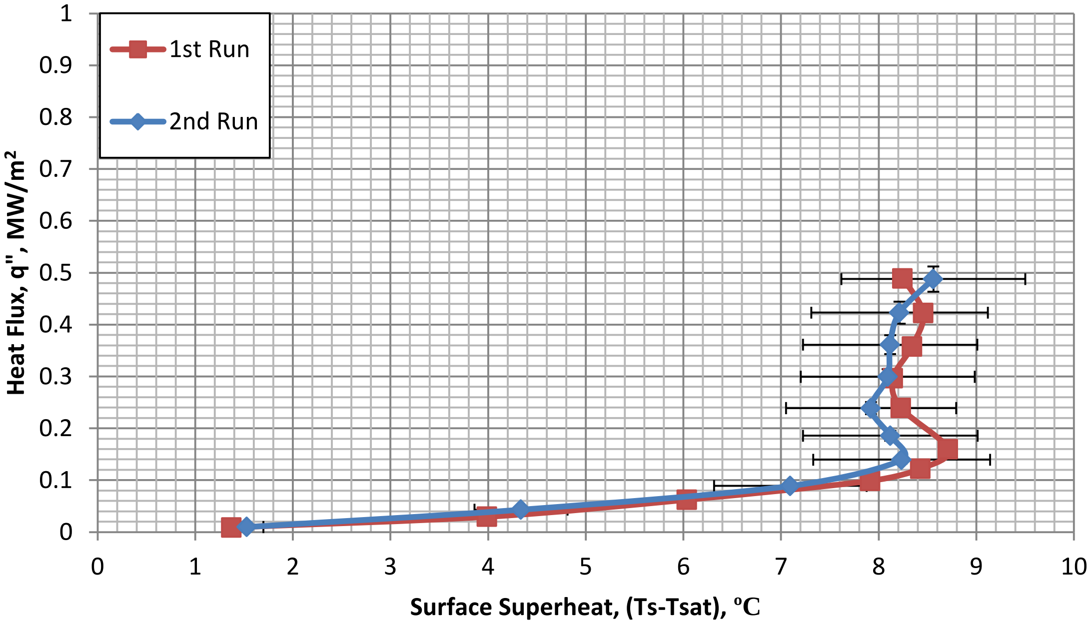

Figure 3.11: Repeatability of surfactant solution boiling curves on the rough boiling surface.

Chapter 4 Results and Discussion

The results of the nanofluid and deionized water pool boiling experiments carried out in this experimental investigation are provided and discussed in this chapter. Each stage of experiments is discussed separately. Stage 1 focused on investigating the effect of the heated surface roughness. Stage 2 focused on investigating the effect of nanoparticles concentration and surfactants concentration. The isolated bubbles formation and bubbles growth rates of pure water and nanofluids were studied in Stage 3.

4.1 Stage 1: Effects of the Heated Surface Texture and Surface Roughness

In stage 1 of experiments, the first heated surface configuration was used. The boiling surfaces have been prepared and machined to a mirror surface finish using diamond turning machine. Deionized water and nanofluids were boiled on the smooth and rough surfaces, with an average surface roughness of 6 and 60 nm, respectively. Nanofluids at 0.05 wt. % concentration and 0.1 wt. % of SDBS were used at this stage. A summary of the experiments conducted at this stage is shown in Table 4.1. The surfactant concentration used is the critical micelle concentration (CMC) [35]. This concentration of surfactant was reported to enhance the nanoparticles suspension and reduce nanoparticles agglomeration [11], [32], [33]. The boiling curves of water and nanofluids obtained using the smooth and rough surfaces are shown in Figure 4.1.

Table 4.1: Details of boiling experiments carried out during Stage 1.

Designation	**Working Fluid Composition**	**Ra (nm)**	**ONB (°C)**	**HTC ratio w.r.t. water @ 0.5 MW/m^2**	**Performance**
DW6	Deionized Water	6	9	1	---
0.1NPSDBS6	0.05% NP + 0.1% SDBS	6	6.4	2.05	Enhancement
0.1DWNF6	Deionized Water after the nanofluid experiment	6	9.5	1	Same as for the clean surface
DW60	Deionized Water	60	7.5	1	---
0.1NPSDBS60	0.05% NP + 0.1% SDBS	60	9	0.88	Deterioration
0.1DWNF60	Deionized Water after the nanofluid experiment	60	10	0.61	Deterioration

In natural convection regime, the boiling curves of pure water show heat transfer enhancement with the increase of the surface roughness. Also, the boiling curves of nanofluids show a similar trend of enhancement with the increase of the surface roughness. The nanofluids heat transfer enhancement can be attributed to the thermal conductivity increase with the addition of nanoparticles as reported by several researchers [2], [5], [6]. In the nucleate boiling regime, the same trend of increase in the heat transfer rate with the increase in the surface roughness is observed for the case of pure water. In the case of pure water, the onset of nucleate boiling (ONB) is decreased from 9 ºC of wall superheat for the smooth surface to 7.5 ºC for the rough surface.

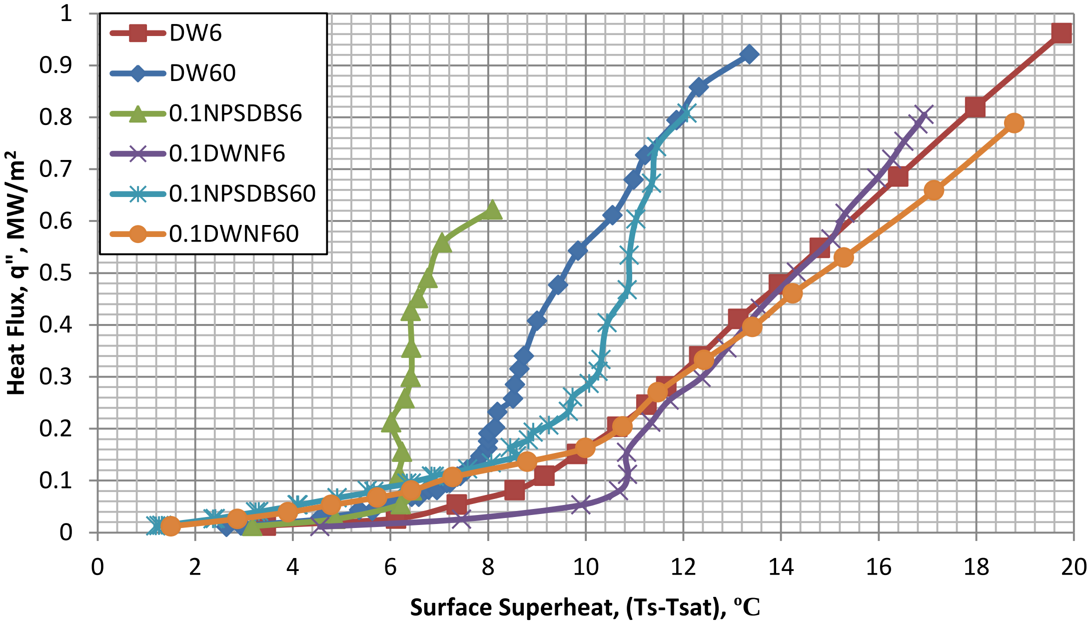

Figure 4.1: Boiling curves obtained during experiments of stage 1.

Mixed results of both heat transfer enhancement and deterioration are observed for the case of nanofluids. In the case of the rough surface (Ra = 60nm), a deterioration in the nanofluids heat transfer rate compared to pure water is observed. The heat transfer coefficient (HTC) decreased by about 10% with respect to pure water. The HTC has been calculated at a constant heat flux of 500 KW/m^2. Visual inspection of the boiling surface after the nanofluids boiling experiment showed a thick layer formed on the surface that was observed by the naked eye. The image of the boiling surface after the nanofluids boiling experiment is shown in Figure 4.9 (c). This layer could not be removed using a water jet. The surface had to be re-machined for the next experiment. The performance of the nanoparticles deposited surface was examined by carrying out another pure water boiling experiment. The obtained boiling curve showed heat transfer deterioration with respect to the original boiling curves of water and nanofluid on clean surfaces. The HTC decreased by about 40% with respect to pure water boiling on a clean surface. The heat transfer deterioration can be attributed to the formation of the nanoparticles deposition layer. This layer is found to add thermal resistance to the surface and block some active nucleation sites that reduced the rates of heat transfer eventually. It is also noticed that the surfactant failed to provide good suspension of the nanoparticles and stop the deposition process on the heated surface.

The results of this stage showed disagreement with the findings of Narayan et al. [16]. According to their hypothesis, the SIP value for the rough surface is equal to 6, which is much larger than unity and therefore nanofluid heat transfer enhancement is expected, which did not actually happen, although surfactant was added to improve the stability of the nanofluid.

For the smooth surface (Ra = 6nm), nanofluid nucleate boiling showed very high heat transfer enhancement with respect to deionized water. It can be seen that a fractional increase in the surface superheats results in very high heat transfer increase. The nanofluid heat transfer coefficient (HTC) is increased twice with respect to deionized water at the same roughness level and at a medium heat flux of 500 KW/m^2. It can be easily observed from the increase in the slope of the boiling curve. The high-speed images of the boiling phenomena of pure water and nanofluid captured at different surface heat fluxes are shown in Figure 4.3. These images reveal that the size of the bubbles developed during the nanofluid boiling is much smaller than those of pure water. The reduced surface tension in the case of the nanofluid, due to the presence of the surfactant, caused the observed reduction in the bubbles size according to the Laplace equation *44.1*.

$$P_g - P_f = \frac{2\,\sigma}{r_{nuc}} \qquad 44.1$$

The smaller bubble size reduces the bubble growth time according to Equation 2.5 reported by Plessent and Zwick [22]. Therefore, bubble nucleation frequency increases significantly which in turn increases the surface rewetting with the nanofluid and reduces the required wall superheat. The heat transfer enhancement is combined with a decrease in the ONB from 9 to 6.4 ºC.

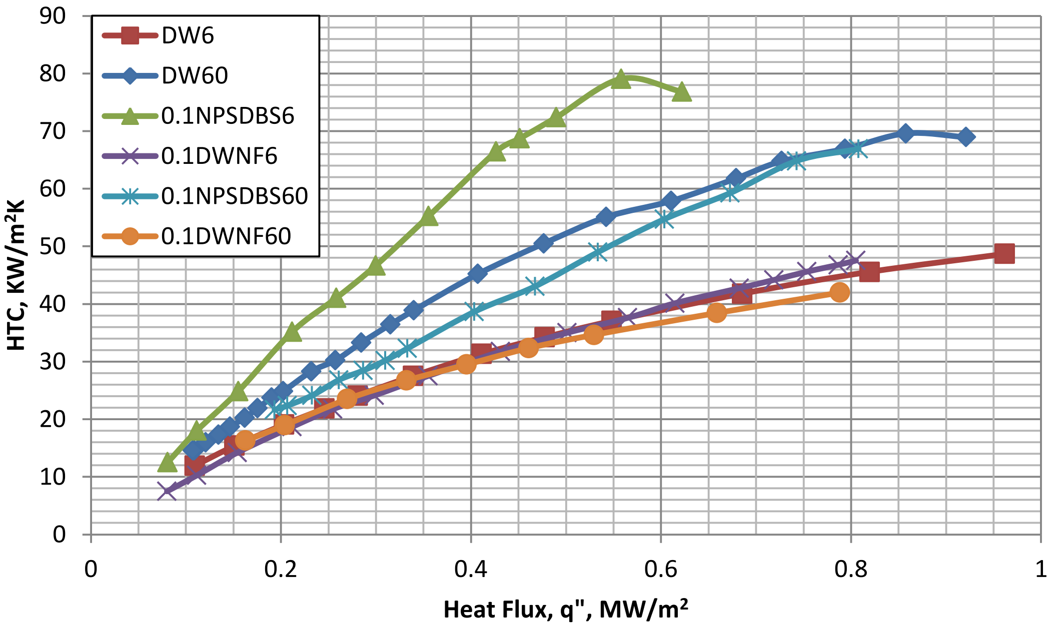

Figure 4.2: Heat transfer coefficient of different working fluids calculated from various experiments carried out in stage 1.

The image of the boiling surface after the nanofluids boiling experiment is shown in Figure 4.9 (d). Deionized water boiling experiment on the smooth surface produced from the nanofluid boiling experiment shows very similar performance to the deionized water boiling curve on a clean surface. This conclusion confirms that no nanoparticles deposition existed on the smooth surface. Critical heat flux (CHF) values for deionized water experiments on clean surfaces of 6 and 60 nm average surface roughnesses are around 950 kW/m^2.

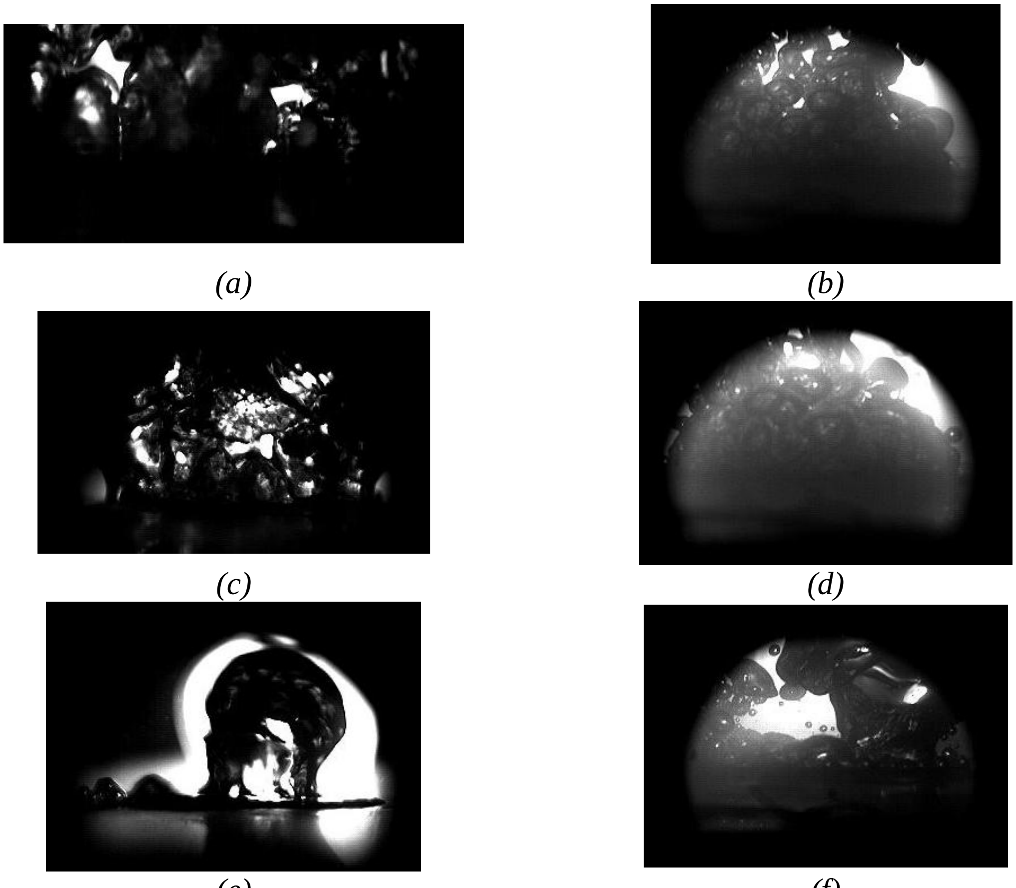
(a) *(b)*
(c) *(d)*
(e) *(f)*

Figure 4.3: Images of deionized water and nanofluid boiling at different heat fluxes of: (a) water at 200 KW/m2, (b) nanofluid at 200 KW/m2, (c) water at 400 KW/m2, (d) nanofluid at 400 KW/m2, (e) water at CHF and (f) nanofluid at CHF.

4.2 Stage 2: Effects of Nanofluid Concentration and Surfactant Concentration.

Due to the mixed nanofluid boiling performance of enhancement and deterioration observed on the smooth and on the rough surfaces, respectively, the effect of the nanofluid and surfactant concentration needed to be investigated separately. Two surfactant concentrations of 0.1 and 1.0 wt. % have been tested using the rough surface. The nanoparticles concentration was kept constant at 0.05 wt. %. The effects of the nanofluid concentration have been examined by carrying out experiments using the smooth boiling surface with two nanofluid concentrations of 0.05 and 0.1 wt. %. The first heated surface configuration was used in all experiments carried out at this stage.

4.2.1 Effect of Surfactant Concentration on the Rough Surfaces

Table 4.2: Details of boiling experiments carried out on the rough surface (Ra = 60nm).

Designation	**Working fluid Composition**	**Ra (nm)**	**ONB (^{o}C)**	**HTC ratio w.r.t. water @ 0.5 MW/m^2**	**Performance**
DW60	Deionized Water	60	7.5	1	-
0.1NPSDBS60	0.05% NP + 0.1% SDBS	60	9	0.88	Deterioration
0.1DWNF60	Deionized Water after the 0.05% NP + 0.1% SDBS nanofluid experiment	60	10	0.61	Deterioration
1.0NPSDBS60	0.05% NP + 1.0% SDBS	60	6.4	1.34	Enhancement
1.0DWNF60	Deionized Water after the 0.05% NP + 1.0% SDBS nanofluid experiment	60	8.4	1	Same as for the clean surface

Figure 4.4 presents the boiling curves obtained for nanofluids with two different surfactant concentrations. The boiling experiments were carried out using the rough

surface (Ra = 60 nm). Details of the boiling experiments conducted are listed in Table 4.2. The boiling curve obtained for the case of nanofluid with 1.0 wt. % surfactant showed heat transfer enhancement with respect to the pure water boiling curve obtained using the same surface. This boiling curve is very similar in trend to the nanofluid boiling curve obtained using the smooth surface, discussed in section 4.1. The boiling HTC is 34% higher than that of pure water. The ONB occurred at a lower wall superheat of 6.4 ºC. Similar to the nanofluid boiling curve on the smooth surface, discussed in section 4.1, visual inspection showed that the nanofluid boiling has altered the heated surface condition, as shown in Figure 4.9 (e). However, the pure water boiling performance on this surface produced very similar characteristics to the boiling on the clean surface. Figure 4.5 shows the boiling HTC of different working fluids. There is no appreciable difference in the HTC between the two pure water experiments.

Reducing the surfactant concentration to 0.1 wt. % had a negligible effect on the heat transfer rate in the natural convection regime. Unfavorably, the ONB shifted to a higher wall superheat of 9 ºC. Also, heat transfer deteriorations occurred in the nucleate boiling regime. The HTC decreased by 12 % with respect to pure water. Although the reduction in the HTC of the nanofluid was small, the nanofluid boiling curve was found to lay outside the margin of error of the pure water boiling curve. This deterioration is accompanied by the formation of a heavy nanoparticles deposition layer on the surface. A degradation in deionized water boiling performance on the deposited surface by 40% was observed.

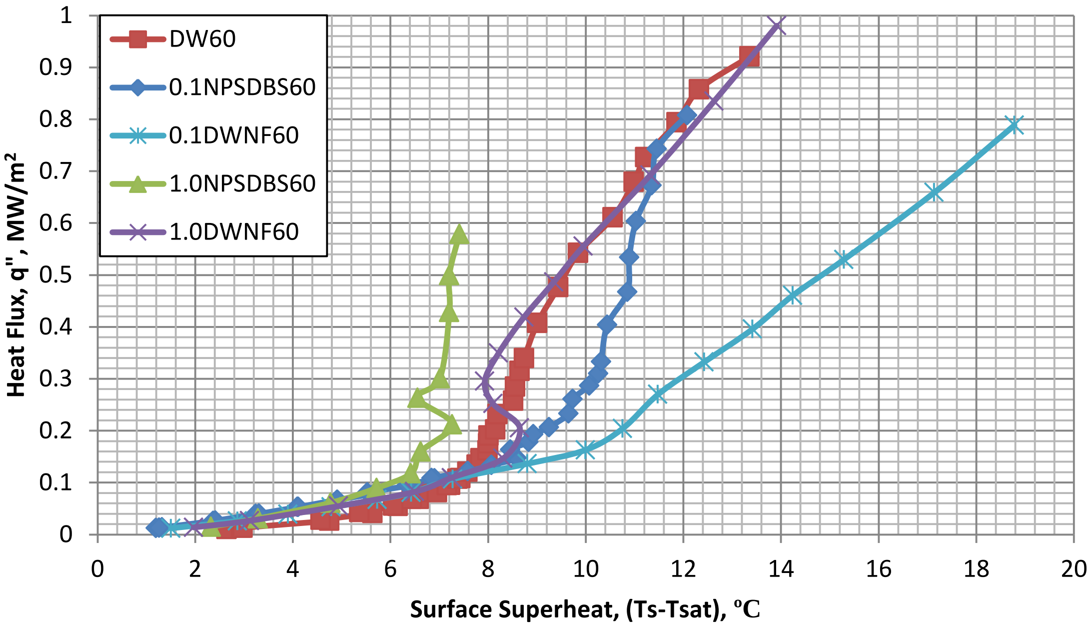

Figure 4.4: Boiling curves of nanofluids with different surfactant concentrations on a rough surface with Ra = 60 nm.

The effects of the addition of dispersants to nanofluid mixtures showed contradicting performance in the literature. Chopkar at al. [14] concluded that the mixture of ZrO_2 and surfactant deteriorated the boiling heat transfer even though heat transfer enhancement was achieved by the surfactant solution as shown in Figure 2.7. Tang et al [13] and Kathiravan et al. [15] found that nanofluid heat transfer enhancement increased with the addition of surfactant. The difference between the boiling performances of nanofluids due to the different concentration of surfactants proved that the surfactant can achieve nanofluid boiling heat transfer enhancement regardless of the roughness of the boiling surface. Results show that there is a threshold surfactant concentration for every surface roughness beyond which nanofluid heat transfer enhancement is obtained. The threshold surfactant concentration is responsible for two factors that enhance the nanofluid boiling heat transfer.

The first factor is the existence of surfactant micelles. Surfactants form micelles when the surfactant concentration exceeds the CMC value [35]. In aqueous surfactant solution above CMC, the hydrophobic tails, which are the non-wetting part, form the core of the micelle and the hydrophilic heads, which are the wetting part, are in contact with the surrounding liquid. When the nanoparticles are added to the solution, the micelles are reformed around the nanoparticles where the nanoparticles are in the micelle’s core and surrounded with the hydrophobic tails. The nanoparticles suspension and consequently the nanofluid stability are increased. Increasing the surfactant concentration increases the number of micelles formed in the bulk liquid which increases the amount of nanoparticles lifted up by the micelles and prevents the possibility of nanoparticles deposition.

The second factor is the reduction of actual nanoparticles size in suspension with the increase of surfactant concentration. Figure 4.8 shows the actual size of nanoparticle clusters in suspension at different surfactant concentrations measured by the dynamic light scattering (DLS) machine as described in section 3.5. At surfactant concentration of 0.1 wt. %, the average nanoparticles size is 396 nm. This size is reduced by 44% with the increase of surfactant concentration to 1.0 wt. %. The addition of surfactants is found to increase the repulsive forces between the particles to overcome the attractive forces of London-van der Waals as explained by [11].

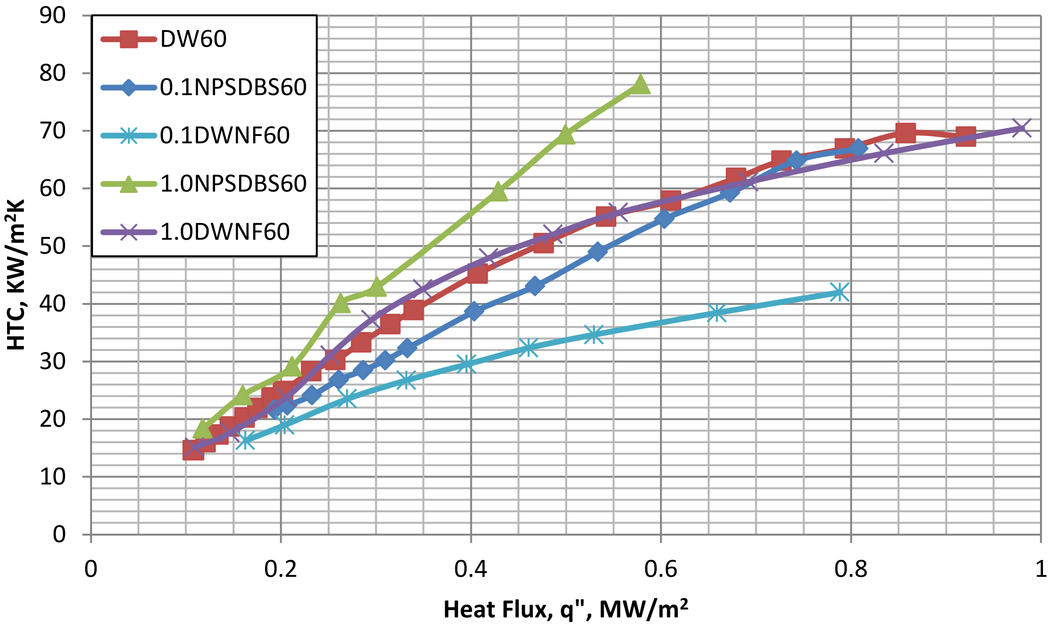

Figure 4.5: Heat transfer coefficient of different working fluids conducted on a rough surface with Ra = 60nm.

The surfactant concentration increase is indirectly responsible for the nanofluid thermal conductivity enhancement. As discussed earlier, the increase of surfactant concentration causes a reduction in the size of actual nanoparticles cluster in suspension. The decrease in nanoparticles size is found to increase the nanofluid thermal conductivity enhancement ratio by [7], [36]. In order to quantify the contribution of the components used in the nanofluid preparation, a boiling experiment of water-surfactant solution at a concentration of 1.0 % on a surface is conducted.

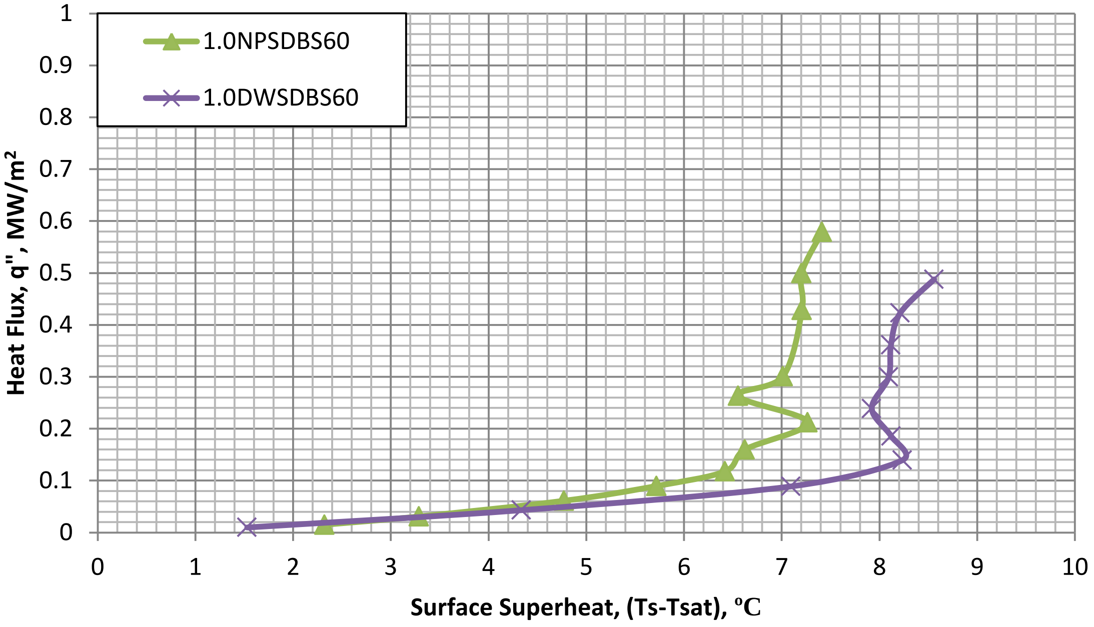

Figure 4.6: Boiling curves of nanofluid with 1% surfactant concentration and 1% surfactant aqueous solution on the rough surface with Ra = 60nm.

The boiling curves of both fluids exhibit a similar trend as shown in Figure 4.6. The surfactant boiling curve confirms that low surface tension is the cause of the high steepness of the boiling curve. The presence of the nanoparticles in suspension caused a shift in the boiling curve to the left. The ONB is decreased from 8.3 ºC of wall superheat to 6.3 ºC. The HTC enhancement ratio of surfactant solution is estimated a value of 11% with respect to pure water. The HTC enhancement ratio contributed by the nanoparticles only are equal to 23%.

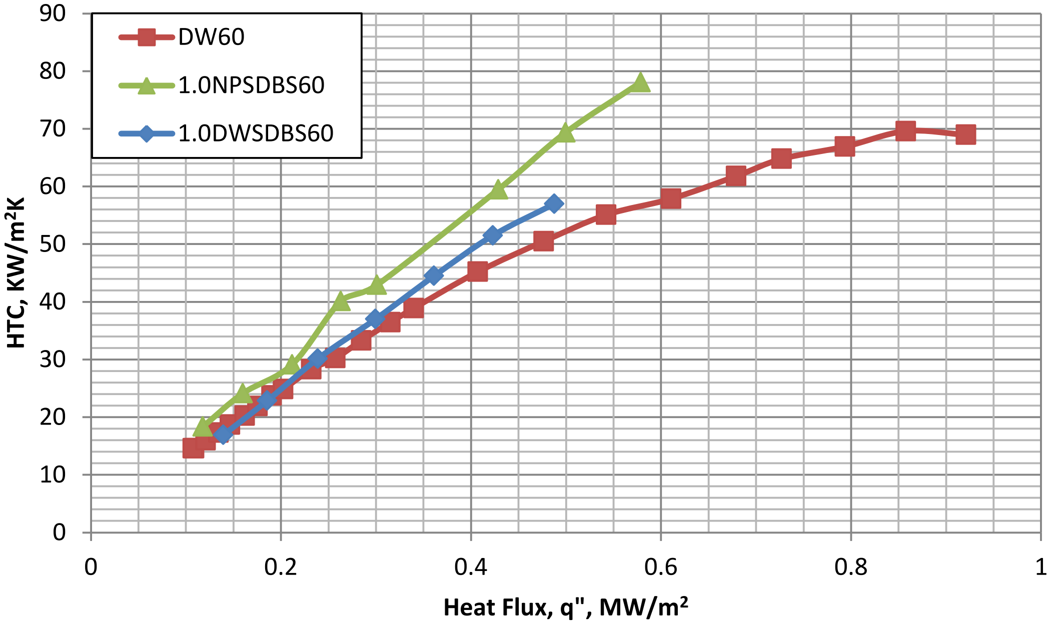

Figure 4.7: Heat transfer coefficient of nanofluid with 1% surfactant concentration and 1% surfactant aqueous solution compared to pure water on the rough surface with Ra = 60nm.

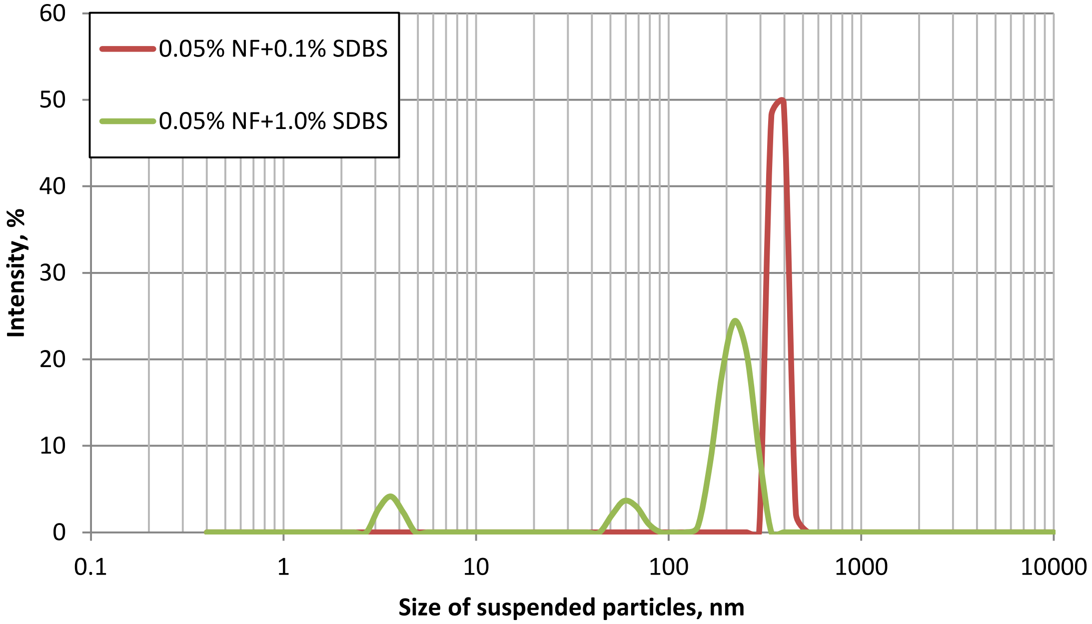

Figure 4.8: Actual nanoparticles size distribution in two nanofluids with different surfactant concentrations.

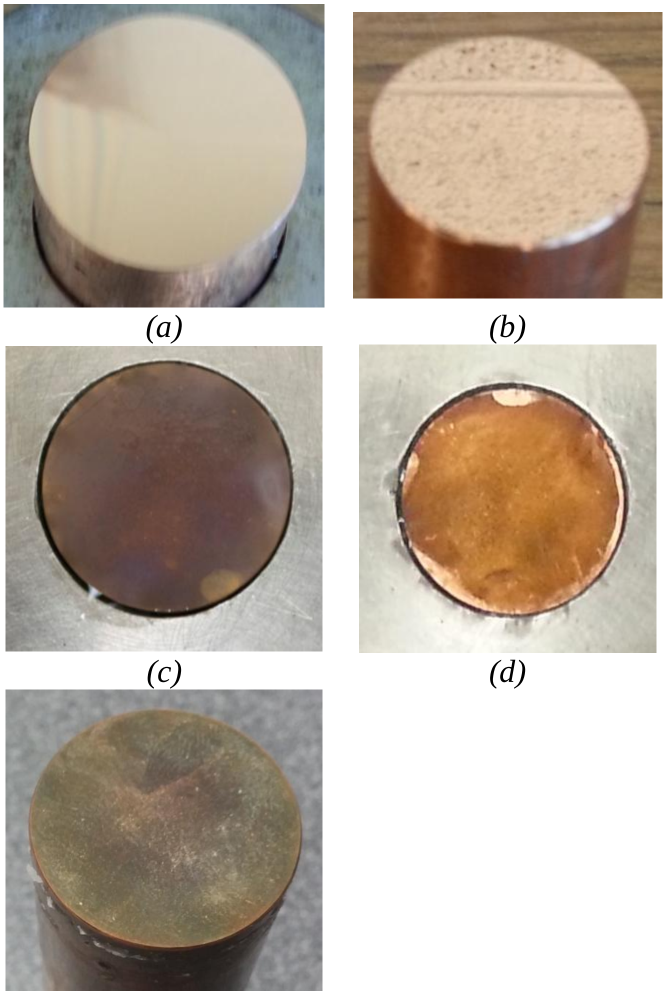

(a) *(b)*

(c) *(d)*

(e)

Figure 4.9: Images of the heated surface after boiling of different working fluids :(a)Clean rough boiling surface, (b)Clean smooth boiling surface, (c)Rough boiling surface after the 0.1NPSDBS60 experiment, (d)Smooth boiling surface after 0.1NPSDBS6 experiment and (e) Rough boiling surface after the 1.0NPSDBS60 experiment.

4.2.2 Effect of Nanofluid Concentration on the Smooth Surface

Table 4.3: Details of boiling experiments carried out on the smooth surface (Ra = 6nm).

Designation	**Working fluid Composition**	**Ra (nm)**	**ONB (ºC)**	**HTC ratio w.r.t. water @ 0.5 MW/m^2**	**Performance**
DW6	Deionized Water	6	9	1	-
0.05NP6	0.05% NP + 0.0% SDBS	6	9.2	1.3	Enhancement
0.05DWNP6	Deionized Water after the 0.05% NP + 0.0% SDBS nanofluid experiment	6	10	1.027	-
0.1NP6	0.1% NP + 0.0% SDBS	6	10	1.11	Enhancement
0.1DWNP6	Deionized Water after the 0.1% NP + 0.0% SDBS nanofluid experiment	6	10	0.94	-

Unlike the boiling heat transfer deterioration encountered by the nanofluid with surfactant on the rough heated surface, the same nanofluid composition gave heat transfer enhancement on the smooth as presented in 4.1. In order to understand the nanofluid boiling on smooth heat surfaces, two nanofluids with different nanoparticles concentration are investigated. No surfactant is used in this part of the research. Figure 4.10 presents the boiling curves for nanofluids experiments done. Details of the boiling experiments conducted are listed in Table 4.3.

The 0.05 wt. % nanofluid exhibits very high heat transfer rates with respect to deionized water in both natural convection and nucleate boiling regimes. The nanofluid HTC reaches a value of 48 KW/m^{2}K while the water HTC is 36 KW/m^{2}K at a medium heat flux of 0.5 MW/m^2 as shown in Figure 4.11. It represents a 30% increase in the nanofluid HTC. There is a little change in the ONB between the water and nanofluid which occurs at wall superheat of 9.2 ºC.

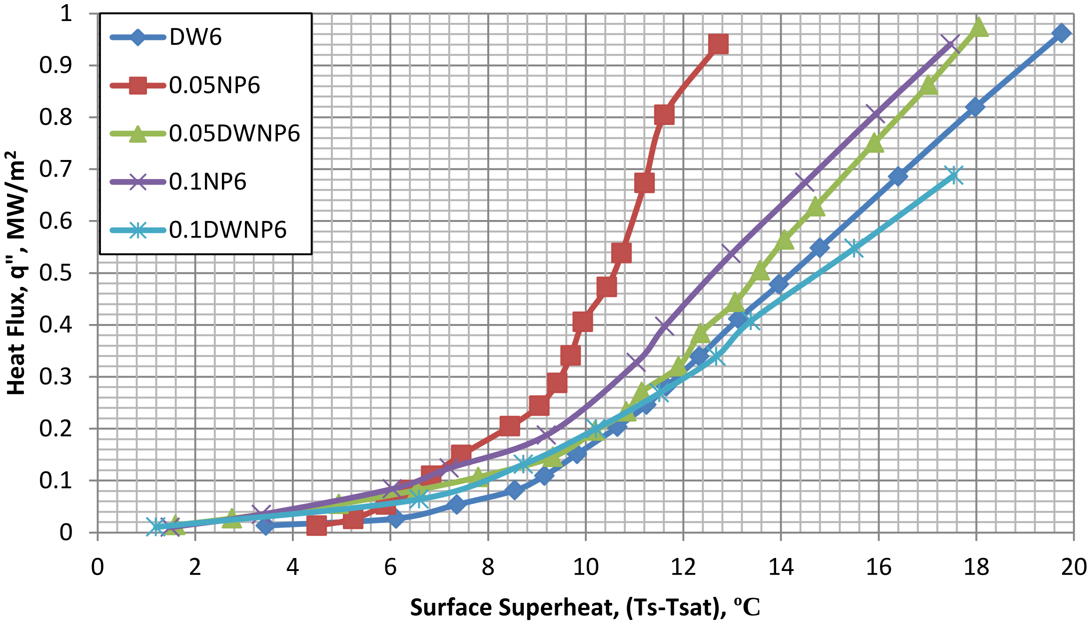

Figure 4.10: Boiling curves of nanofluids with different nanoparticles concentrations on a smooth surface with Ra = 6 nm.

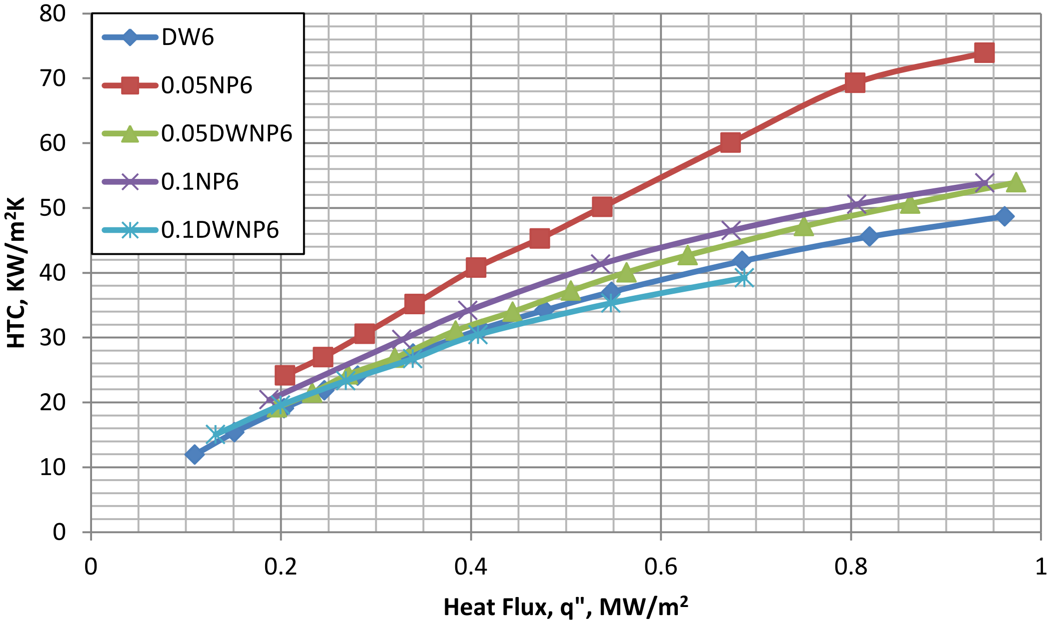

Figure 4.11: Heat transfer coefficient of different working fluids conducted on a rough surface with Ra = 6nm.

Comparison of the nanofluid boiling performance at the same nanoparticles concentration of 0.05 wt. % and smooth heated surface with and without the surfactant addition show that the percentage of heat transfer enhancement contributed by the surfactant is higher than the nanoparticles. The effect of surfactant is clearly seen by the large reduction in ONB from 9.2 to 6.4 ºC and the steepness of the boiling curves in stages 1 and 2 due to its low surface tension. The adsorption layer formed by the surfactant [37] prevented the formation of the nanoparticles deposition layer. The surfactant caused a large reduction in CHF as it is confirmed by the work of [38], [39]. Kathiravan et al. [15] reported that the CHF of the nanofluid with surfactant reached one-third the CHF value of the nanofluids only.

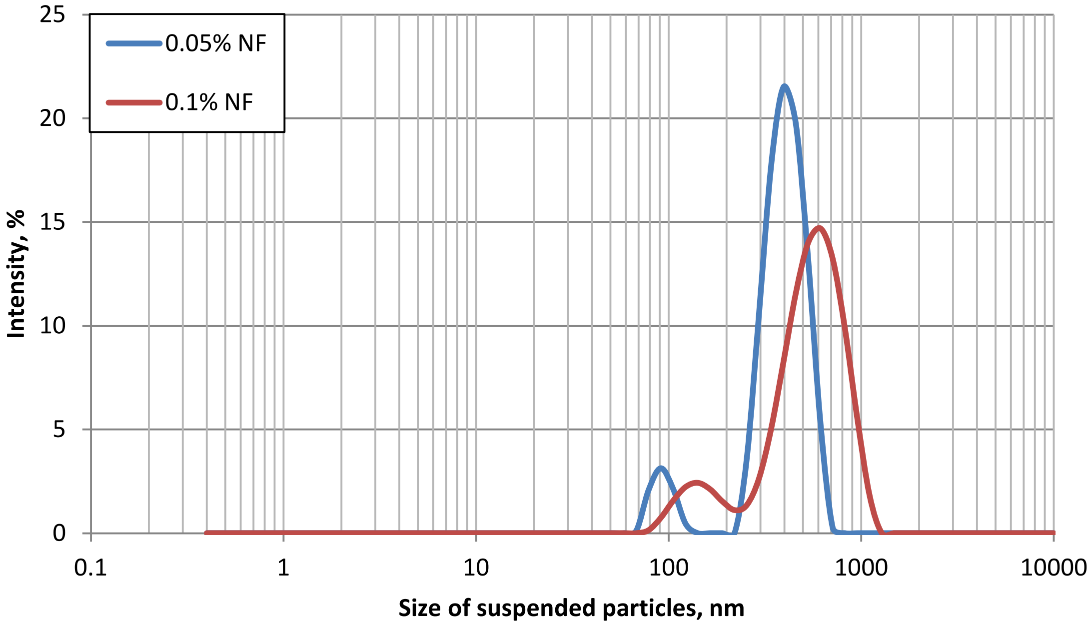

Figure 4.12: Actual nanoparticles size distribution in two nanofluids with different nanoparticles concentrations.

Increasing the nanoparticles concentration to 0.1 wt. % also causes boiling heat transfer enhancement compared to deionized water. However, the heat transfer enhancement decreases with the increase of nanoparticles concentration. The boiling HTC enhancement ratio of nanofluid at the 0.1 wt. % concentration is 11% with respect to pure water. This trend has been confirmed many researchers [13]–[16], [18]. The ONB for the higher nanofluid concentration increases by 1 ºC. It was expected that the increase in nanoparticles concentration will lead to increase in heat transfer enhancement. The measurement of actual nanoparticles size for both concentrations in Figure 4.12 reveals that higher average nanoparticles' size is associated with the higher concentration. This increase of nanoparticles actual size caused the decrease of thermal conductivity of nanofluid at the high concentration which returned lower heat transfer enhancement [7], [36] as presented in Figure 4.10. The performance of pure water on surfaces produced from the nanofluids boiling experiments show very similar boiling performance to pure water performance on a clean surface.

The nanofluid boiling results contradict the findings of Kwark et al. [12] who tested a dilute nanofluids with a similar volumetric concentrations of 0.0125 and 0.025 % and reported that the boiling curves of these nanofluid were similar to the pure water boiling curves with deterioration occurred at high heat fluxes. The deterioration increased with the nanoparticles concentrations. The nanoparticles attributed to increase the CHF of the mixtures from 1010 to 1980 KW/m^2. These results are justified by the effect of the interactions between the nanoparticles and the boiling surface. Wen at al. [17] found that nanofluid with volumetric concentration of 0.0001 % achieved heat transfer enhancement on the smooth boiling surface whereas it achieved the same boiling performance as the pure water on the rough surface.

Again, the predictions of Narayan et al. [16] are opposite the results of this stage. Calculating the SIP parameter of the smooth surface which is equal to 0.6 predicted that boiling heat transfer deterioration as the nanoparticles will block the active nucleation sites that have similar sizes. There are several reasons that cause such contradiction. First, the nominal particle size is used instead of the actual size of the nanoparticles in suspension as claimed by Wen et al. [17]. In addition, the results are affected by the heating surface shape and orientation. They used a vertical tube as a heating surface. This configuration minimized the effects of nanoparticles deposition on the heated surface and modified the heat transfer due to the bubble sliding on the surface. The inconsistency of the surface texture is due to the surface preparation method and the heater shape.

4.3 Stage 3: Isolated Bubbles Formation and Bubbles Growth Rates.

In this stage, the growth of single isolated bubble has been observed and compared to the case of pure water and the case of nanofluid. A single concentration of 0.05 wt. % of nanofluids has been used with no surfactant added to avoid multiple bubbles generation as reported in [40]. The second heated surface configuration has been used to avoid multiple bubbles generation at different locations on the surface. The boiling surface has been hand polished to an average surface roughness of 120 nm.

Images of the growing bubble in deionized water captured by using the high-speed camera are shown in Figure 4.13. One can observe that the shape of the bubbles is not spherical. Hetsroni et al. [40] found that the bubbles grew using the natural roughness of stainless steel foil have a non-spherical shape that is horizontally axisymmetric and vertically asymmetric.

The bubble growth rate in the case of deionized water at different wall superheats is shown in Figures 4.14 to 4.16. The growth rates are fitted to an empirical power law equation, and the resulting power varies between 0.32 and 0.37. These results are in reasonable agreement with the theoretical models reported in [22], [23].

These models assumed a spherical bubble growing in a superheated layer with a uniform temperature existing above the heated surface. Past research concluded that the actual bubble shape is not spherical. Siedel et al. [31] reported that the shape of the bubbles growing from the artificial cavity is not spherical. Also, temporal and spatial temperature variations around the bubble nucleation site were experimentally verified by means of IR thermography in [28] as shown in Figure 2.12. The performance of the theoretical model expects that lower growth rate occurs prior to detachment however the actual growth rate remained unchanged. Figure 4.14 shows that the results of Gerardi et al. [28] possess the same trend discussed. This theoretical performance is only coupled with the nucleation with an artificial cavity because of the large volume of vapor trapped inside of it.

Other parameters of the bubble nucleation process are in conformance with the literature findings. The bubble departure diameter increases with the wall superheat and reaches a maximum radius of 2.3 mm. The bubble waiting time significantly reduces with the increase of wall superheat and consequently the nucleation frequency increases with the wall superheat. The relationships of bubble departure diameter and nucleation frequency are presented in Figures Figure 4.18 and Figure 4.19 respectively.

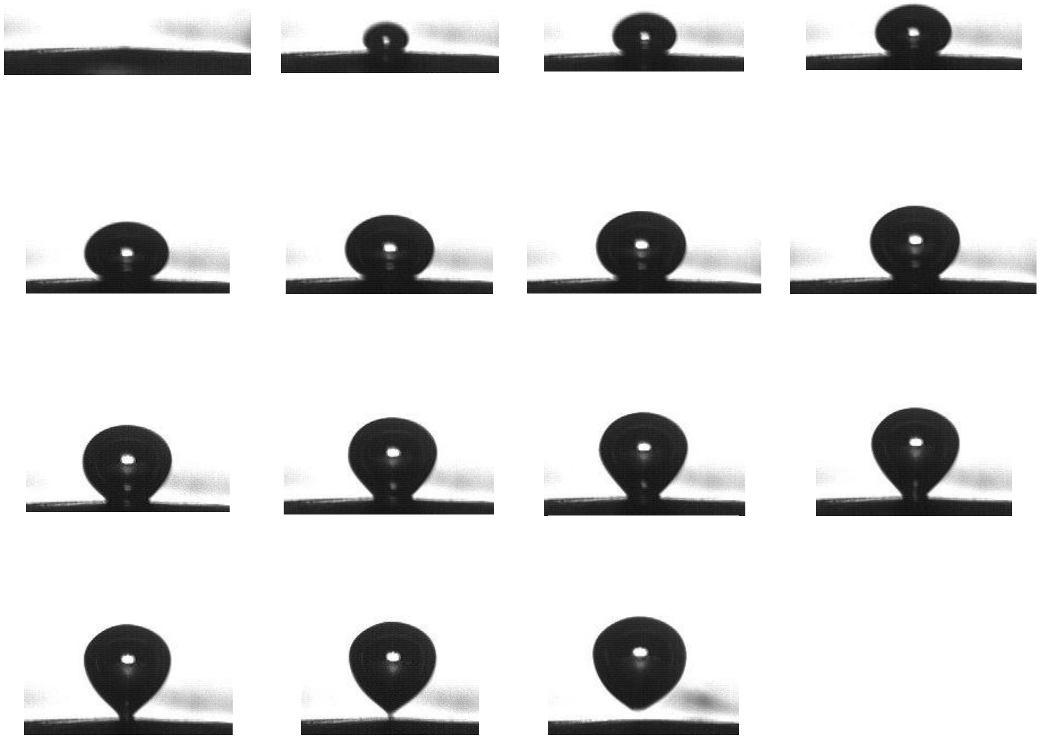

Figure 4.13: Images of the growing water bubble taken 1 ms apart at wall superheat of 104 ºC.

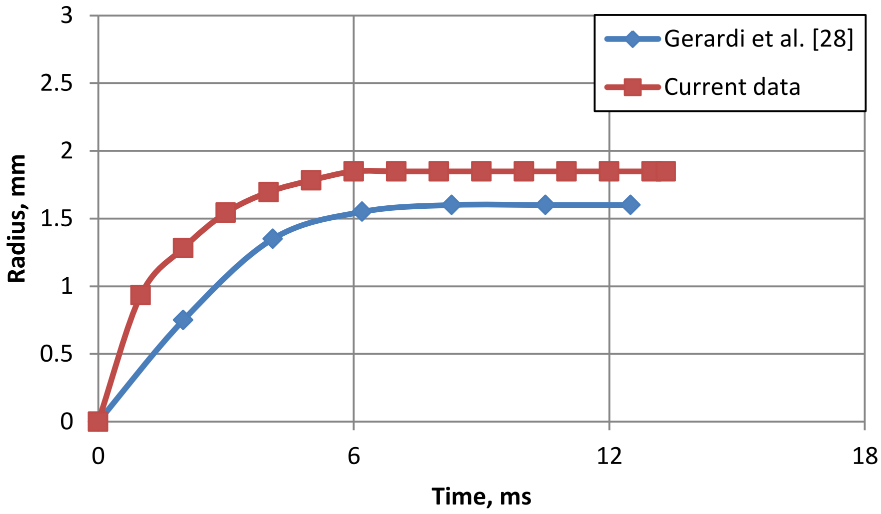

Figure 4.14: Comparison of the current bubble growth rate with the one reported in [28] *in the case of pure water.*

The nucleation process of nanofluid is quite different from the deionized water. Although, the same experimental setup, the same boiling surface and the same tip area of the conical heating element are used, many nucleation sites were activated in the same small local heated area instead of one observed in the case of pure water, as depicted in Figure 4.20. The bubbles generated in the nanofluid are more spherical. They are much smaller in size with respect to the bubbles observed in the case of pure water. The bubble growth rates at different wall superheats are presented in Figures Figure 4.21 and Figure 4.22.

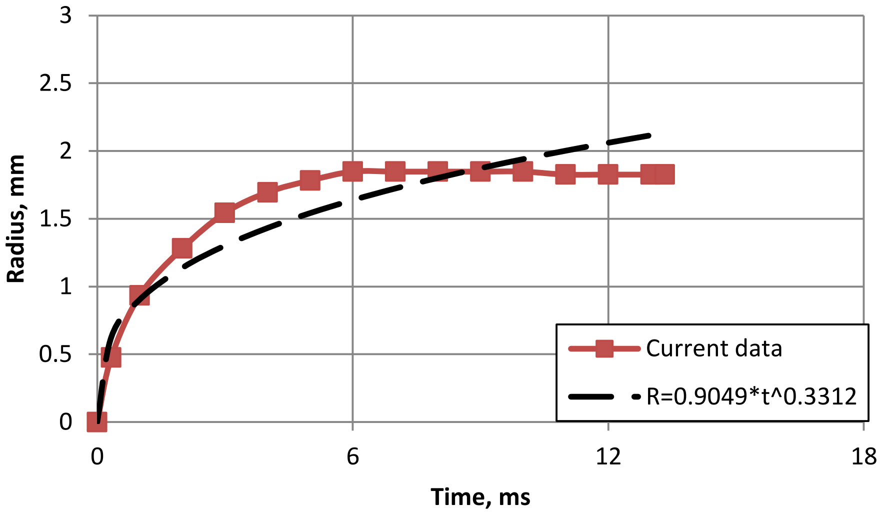

Figure 4.15: Bubble growth rate in the case of pure water at wall superheat of 104.37 ºC.

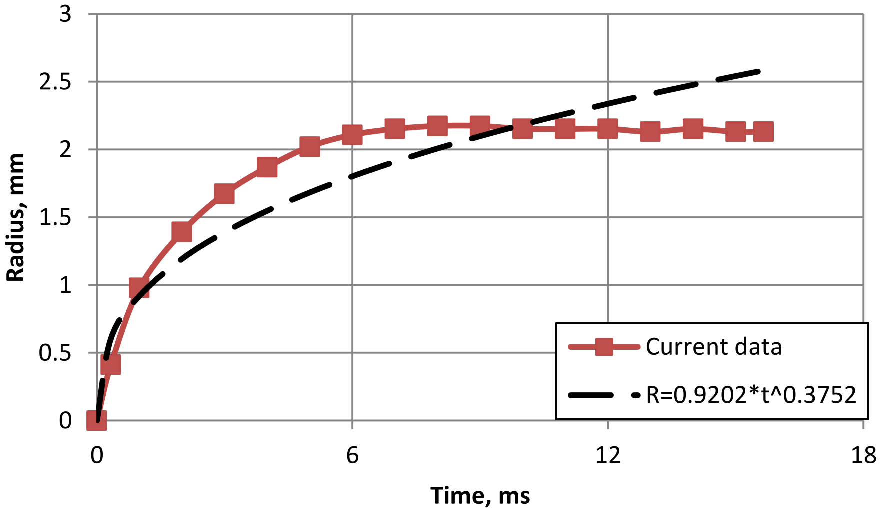

Figure 4.16: Bubble growth rate in the case of pure water at wall superheat of 105.09 ºC.

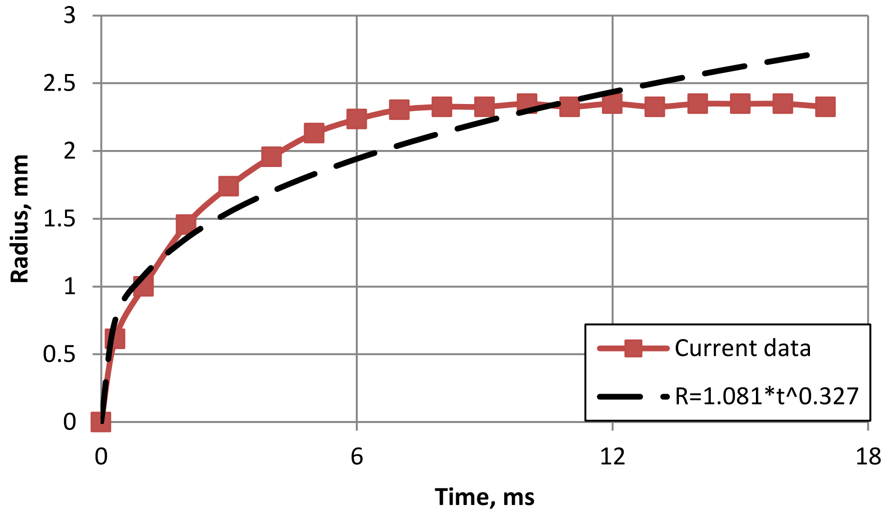

Figure 4.17: Bubble growth rate in the case of pure water at wall superheat of 105.94 ºC.

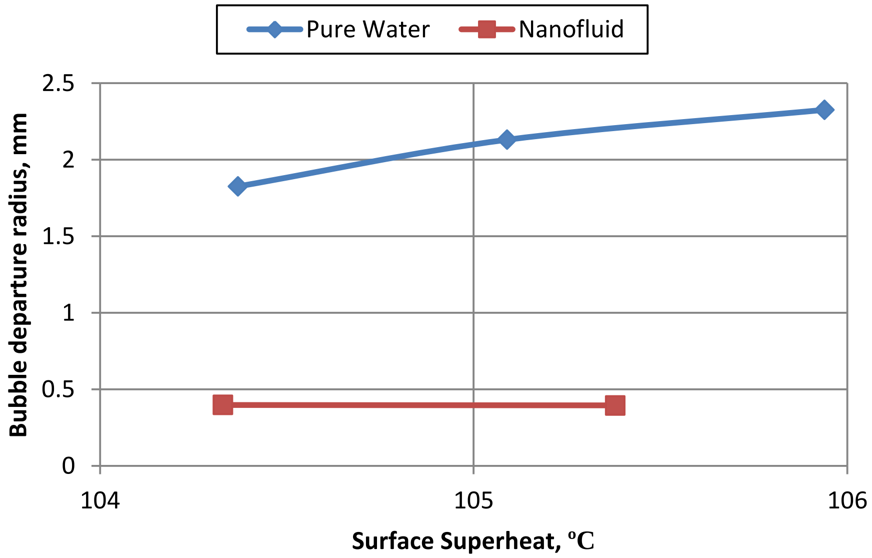

Figure 4.18: Bubble detachment radius as a function of wall superheat.

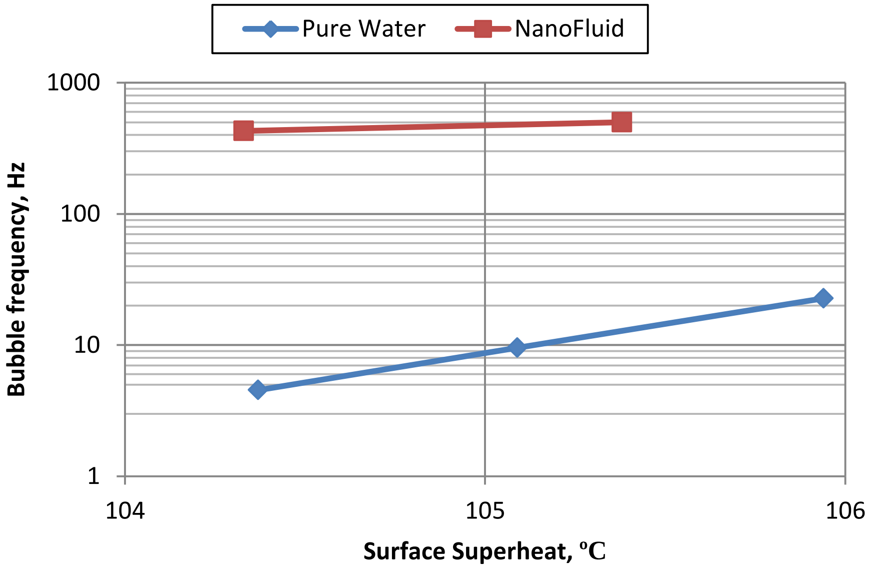

Figure 4.19: Bubble frequency as a function of wall superheat.

The nanofluid bubble growth rates fit very well with the empirical power law equation where the used power varies between 0.38 and 0.41. Because of the smaller bubble sizes in the case of nanofluid, it can be hypothesized that the presence of the nanoparticles caused a reduction in the surface tension according to Laplace Equation *44.1* which in turn caused a reduction in the growth times according Forster and Zuber [23] model. The relationship between the bubble departure diameter and the wall superheat is presented in Figure 4.18. The bubble departure radius does not change with the wall superheat. Comparison of the bubble sizes in deionized water and nanofluid reveals that the bubble radius of nanofluid reduced by 61%. The bubble waiting time is significantly reduced below the time resolution of the measurement. Therefore, the nanofluid bubble nucleation frequency is much higher than pure water. The nucleation frequency reaches 500 Hz at wall superheat of 105.38 ºC.

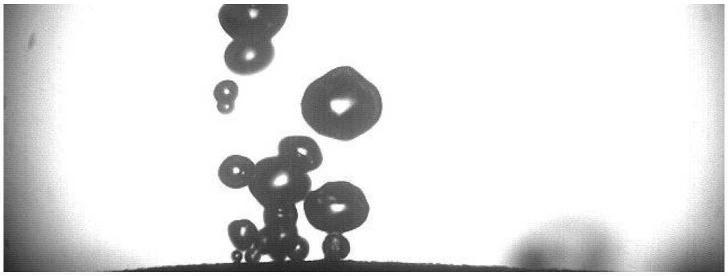

Figure 4.20: Activation of many nucleation sites in nanofluid boiling.

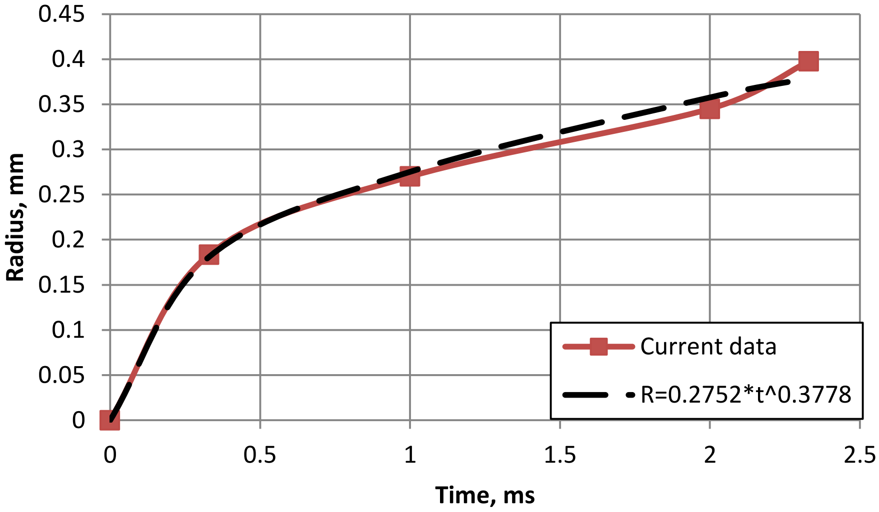

Figure 4.21: Bubble growth rate in the case of nanofluids at wall superheat of 104.33 ºC.

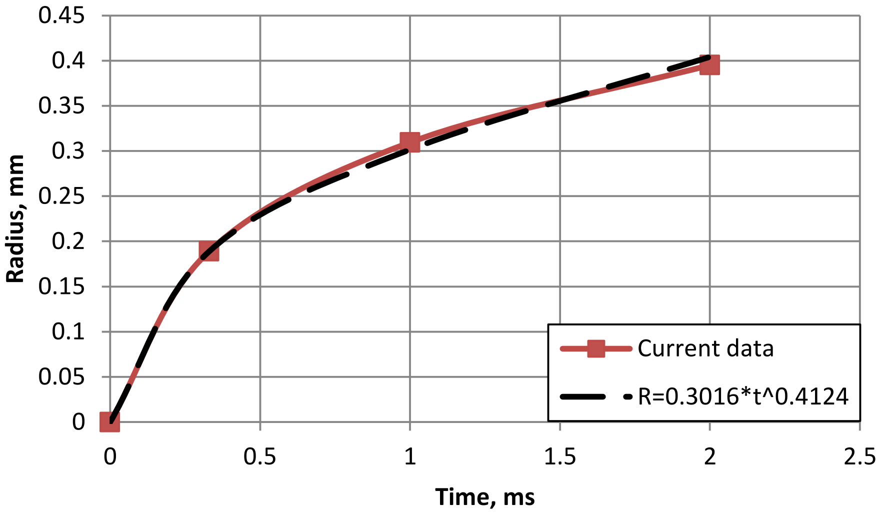

Figure 4.22: Bubble growth rate in the case of nanofluids at wall superheat of 105.38 ºC.

Chapter 5 Summary and Conclusions

An experimental study has been carried out to investigate the effect of some of the suspected parameters that might have contributed to the contradicting results reported in the literature in the case of pool boiling of nanofluids. The effects of the heated surface roughness, surfactant concentration and nanoparticles concentration have been studied. In addition, bubble growth of the isolated bubbles in nanofluids and pure water has been investigated.

Water based nanofluids were prepared using a two-step method from dry alumina oxide nanoparticles with an initial size of 10 nm. The boiling experiments have been conducted on two flat copper surfaces with average surface roughness of 6 and 60 nm. The nanoparticles concentrations used were 0.05 and 0.1 wt. %. The surfactant was also used in this study with two concentrations of 0.1 and 1.0 wt. %. The effect of the surface roughness was studied in the first stage of the current experiments. The second stage focused on the effect of the nanoparticles and surfactant concentrations. Bubble growth was studied in the third stage.

The performance of nanofluids was found to be dependent on the heated surface condition. The nanofluid enhanced the boiling heat transfer in the case of the smooth surface, while it deteriorated the heat transfer on the rough surface. Changing the surfactant concentration greatly altered the nanofluid boiling heat transfer performance. It reduced the deposition of nanoparticles on the heated surface and reduced the actual size of the nanoparticles cluster in the suspensions. For every surface roughness, there is a surfactant concentration which would promote the boiling process. Exceeding such concentration causes the surfactant to dominate the nanofluid boiling by the effect of the reduced surface tension.

In contrast to the findings of [16], which reported heat transfer deterioration using the smooth heated surfaces, heat transfer enhancement using the smooth heated surface was concluded from the current experimental study. In addition, the current study concluded that heat transfer rate decreased with the increase in the nanofluid concentration.

Comparison of isolated bubble formation in the case of pure water and nanofluids revealed that nanofluids caused a reduction in the bubble departure diameter with respect to pure water. Also, they exhibit very high nucleation frequency due to the diminished bubble waiting time.

Chapter 6 Recommendations for Future Work

Nanofluids showed high sensitivity to the boiling surface condition. Mixed results of heat transfer enhancement and deterioration have been observed using the same nanofluid composition on the heated surface having different surface roughness. The performance of nanofluids has to be extended and investigated against higher boiling surface roughness. The surface preparation method should be kept the same in order to exclude the effects of the surface preparation techniques on the nucleation sites density and the randomness of the surface texture.

More work has to be focused on the stability of nanofluids and its effect on the nanofluid boiling performance. The addition of dispersant proved to increase the stability of the nanofluids. The actual size of the nanoparticles in suspension reduced greatly and in turn increased the thermal conductivity of the nanofluids. However, the surfactant alters the thermos-physical properties of the base fluids unfavorably. The change of acidity (pH) of the nanofluids was found to increase the stability and suspension of the nanoparticles [11], [32]. Their results concluded that the basic nanofluids have better stability. The acidity also offers negligible change in the boiling performance of the base fluids [19]. The effect of acidity should be extensively investigated in the wide range of pH scale from 1 to 14.

The effects of different nanoparticles material should be investigated in future. The relative values of the thermal conductivity of the nanoparticles and the heated surface material will make an insight on the role of the deposition layer. It will reveal whether the thermal conductivity of the nanoparticles material contributes to the performance of the deposition layer or the mechanism of nanoparticles deposition is not affected by the material of the nanoparticles. In addition, the effects of size of the nanoparticles should be studied against different boiling surface roughnesses. It will develop a better understanding of the interactions between the nanoparticles and the heated surface.

Bibliography

[1] J. C. Maxwell, *A treatise on electricity and magnetism*, vol. 1. Clarendon press, 1881.

[2] S. U. S. Chol, “Enhancing thermal conductivity of fluids with nanoparticles,” *ASME-Publications-Fed*, vol. 231, pp. 99–106, 1995.

[3] W. Yu, D. M. France, J. L. Routbort, and S. U. S. Choi, “Review and Comparison of Nanofluid Thermal Conductivity and Heat Transfer Enhancements,” *Heat Transfer Engineering*, vol. 29, no. 5, pp. 432–460, May 2008.

[4] X.-Q. Wang and A. S. Mujumdar, “Heat transfer characteristics of nanofluids: a review,” *International Journal of Thermal Sciences*, vol. 46, no. 1, pp. 1–19, Jan. 2007.

[5] N. R. Karthikeyan, J. Philip, and B. Raj, “Effect of clustering on the thermal conductivity of nanofluids,” *Materials Chemistry and Physics*, vol. 109, no. 1, pp. 50–55, May 2008.

[6] C. H. Li and G. P. Peterson, “Experimental Studies of Natural Convection Heat Transfer of Al2O3/DI Water Nanoparticle Suspensions (Nanofluids),” *Advances in Mechanical Engineering*, vol. 2, pp. 742739–742739, Jan. 2015.

[7] T.-P. Teng, Y.-H. Hung, T.-C. Teng, H.-E. Mo, and H.-G. Hsu, “The effect of alumina/water nanofluid particle size on thermal conductivity,” *Applied Thermal Engineering*, vol. 30, no. 14–15, pp. 2213–2218, Oct. 2010.

[8] C. H. Chon, K. D. Kihm, S. P. Lee, and S. U. S. Choi, “Empirical correlation finding the role of temperature and particle size for nanofluid (Al2O3) thermal conductivity enhancement,” *Applied Physics Letters*, vol. 87, no. 15, p. 153107, 2005.

[9] H. A. Mintsa, G. Roy, C. T. Nguyen, and D. Doucet, “New temperature dependent thermal conductivity data for water-based nanofluids,” *International Journal of Thermal Sciences*, vol. 48, no. 2, pp. 363–371, Feb. 2009.

[10] “Surface tension as a function of surfactant concentration.” [Online]. Available: http://www.kruss.de/services/education-theory/glossary/cmc/.

[11] D. Zhu, X. Li, N. Wang, X. Wang, J. Gao, and H. Li, "Dispersion behavior and thermal conductivity characteristics of Al2O3–H2O nanofluids," *Current Applied Physics*, vol. 9, no. 1, pp. 131–139, Jan. 2009.

[12] S. M. Kwark, R. Kumar, G. Moreno, J. Yoo, and S. M. You, "Pool boiling characteristics of low concentration nanofluids," *International Journal of Heat and Mass Transfer*, vol. 53, no. 5–6, pp. 972–981, Feb. 2010.

[13] X. Tang, Y.-H. Zhao, and Y. Diao, "Experimental investigation of the nucleate pool boiling heat transfer characteristics of δ-Al2O3-R141b nanofluids on a horizontal plate," *Experimental Thermal and Fluid Science*, vol. 52, pp. 88–96, Jan. 2014.

[14] M. Chopkar, A. K. Das, I. Manna, and P. K. Das, "Pool boiling heat transfer characteristics of ZrO₂-water nanofluids from a flat surface in a pool," *Heat and Mass Transfer*. Springer-Verlag, 17-Nov-2008.

[15] R. Kathiravan, R. Kumar, A. Gupta, and R. Chandra, "Characterization and Pool Boiling Heat Transfer Studies of Nanofluids," *Journal of Heat Transfer*, vol. 131, no. 8, p. 081902, Aug. 2009.

[16] G. P. Narayan, K. B. Anoop, and S. K. Das, "Mechanism of enhancement/deterioration of boiling heat transfer using stable nanoparticle suspensions over vertical tubes," *Journal of Applied Physics*, vol. 102, no. 7, p. 074317, Oct. 2007.

[17] D. Wen, M. Corr, X. Hu, and G. Lin, "Boiling heat transfer of nanofluids: The effect of heating surface modification," *International Journal of Thermal Sciences*, vol. 50, no. 4, pp. 480–485, Apr. 2011.

[18] G. Harish, V. Emlin, and V. Sajith, "Effect of surface particle interactions during pool boiling of nanofluids," *International Journal of Thermal Sciences*, vol. 50, no. 12, pp. 2318–2327, Dec. 2011.

[19] O. Ahmed and M. S. Hamed, "Experimental investigation of the effect of particle deposition on pool boiling of nanofluids," *International Journal of Heat and Mass Transfer*, vol. 55, no. 13–14, pp. 3423–3436, Jun. 2012.

[20] A. Bejan and A. D. Kraus, *Heat transfer handbook*, vol. 1. John Wiley & Sons, 2003.

[21] Lord Rayleigh, "VIII. On the pressure developed in a liquid during the collapse of a spherical cavity," *Philosophical Magazine Series 6*, vol. 34, no. 200, pp. 94–98, Aug. 1917.

[22] M. S. Plesset, “The Growth of Vapor Bubbles in Superheated Liquids,” *Journal of Applied Physics*, vol. 25, no. 4, p. 493, May 1954.

[23] H. K. Forster, “Growth of a Vapor Bubble in a Superheated Liquid,” *Journal of Applied Physics*, vol. 25, no. 4, p. 474, May 1954.

[24] L. E. Scriven, “On the dynamics of phase growth,” *Chemical Engineering Science*, vol. 10, no. 1–2, pp. 1–13, Apr. 1959.

[25] B. . Mikic, W. . Rohsenow, and P. Griffith, “On bubble growth rates,” *International Journal of Heat and Mass Transfer*, vol. 13, no. 4, pp. 657–666, Apr. 1970.

[26] S. Witharana, B. Phillips, S. Strobel, H. D. Kim, T. McKrell, J.-B. Chang, J. Buongiorno, K. K. Berggren, L. Chen, and Y. Ding, “Bubble nucleation on nano- to micro-size cavities and posts: An experimental validation of classical theory,” *Journal of Applied Physics*, vol. 112, no. 6, p. 064904, Sep. 2012.

[27] C. Hutter, D. B. R. Kenning, K. Sefiane, T. G. Karayiannis, H. Lin, G. Cummins, and A. J. Walton, “Experimental pool boiling investigations of FC-72 on silicon with artificial cavities and integrated temperature microsensors,” *Experimental Thermal and Fluid Science*, vol. 34, no. 4, pp. 422–433, May 2010.

[28] C. Gerardi, J. Buongiorno, L. Hu, and T. McKrell, “Study of bubble growth in water pool boiling through synchronized, infrared thermometry and high-speed video,” *International Journal of Heat and Mass Transfer*, vol. 53, no. 19–20, pp. 4185–4192, Sep. 2010.

[29] Y.-H. Zhao, T. Masuoka, and T. Tsuruta, “Unified theoretical prediction of fully developed nucleate boiling and critical heat flux based on a dynamic microlayer model,” *International Journal of Heat and Mass Transfer*, vol. 45, no. 15, pp. 3189–3197, Jul. 2002.

[30] M. G. Cooper and A. J. P. Lloyd, “The microlayer in nucleate pool boiling,” *International Journal of Heat and Mass Transfer*, vol. 12, no. 8, pp. 895–913, Aug. 1969.

[31] S. Siedel, S. Cioulachtjian, and J. Bonjour, “Experimental analysis of bubble growth, departure and interactions during pool boiling on artificial nucleation sites,” *Experimental Thermal and Fluid Science*, vol. 32, no. 8, pp. 1504–1511, Sep. 2008.

[32] X. Wang, D. Zhu, and S. yang, “Investigation of pH and SDBS on enhancement of thermal conductivity in nanofluids,” *Chemical Physics Letters*, vol. 470, no. 1–3, pp. 107–111, Feb. 2009.

[33] T. Yousefi, E. Shojaeizadeh, H. R. Mirbagheri, B. Farahbaksh, and M. Z. Saghir, “An experimental investigation on the impingement of a planar jet of Al2O3–water nanofluid on a V-shaped plate,” *Experimental Thermal and Fluid Science*, vol. 50, pp. 114–126, Oct. 2013.

[34] “The dependency of the laser intensity on the size of the suspended particle.” [Online]. Available: https://en.wikipedia.org/wiki/Dynamic_light_scattering.

[35] S. K. Hait, P. R. Majhi, A. Blume, and S. P. Moulik, “A Critical Assessment of Micellization of Sodium Dodecyl Benzene Sulfonate (SDBS) and Its Interaction with Poly(vinyl pyrrolidone) and Hydrophobically Modified Polymers, JR 400 and LM 200,” *The Journal of Physical Chemistry B*, vol. 107, no. 15, pp. 3650–3658, Apr. 2003.

[36] K. Khanafer and K. Vafai, “A critical synthesis of thermophysical characteristics of nanofluids,” *International Journal of Heat and Mass Transfer*, vol. 54, no. 19–20, pp. 4410–4428, Sep. 2011.

[37] X.-L. Yin, L.-J. Wan, Z.-Y. Yang, and J.-Y. Yu, “Self-organization of surfactant molecules on solid surface: an STM study of sodium alkyl sulfonates,” *Applied Surface Science*, vol. 240, no. 1–4, pp. 13–18, Feb. 2005.

[38] W.-T. Wu, H.-S. Lin, Y.-M. Yang, and J.-R. Maa, “Critical heat flux in pool boiling of aqueous surfactant solutions as determined by the quenching method,” *International Journal of Heat and Mass Transfer*, vol. 37, no. 15, pp. 2377–2379, Oct. 1994.

[39] W.-T. Wu, Y.-M. Yang, and J.-R. Maa, “Nucleate pool boiling enhancement by means of surfactant additives,” *Experimental Thermal and Fluid Science*, vol. 18, no. 3, pp. 195–209, Nov. 1998.

[40] G. Hetsroni, A. Mosyak, E. Pogrebnyak, I. Sher, and Z. Segal, “Bubble growth in saturated pool boiling in water and surfactant solution,” *International Journal of Multiphase Flow*, vol. 32, no. 2, pp. 159–182, Feb. 2006.